Shifts in the size structure of the microbial community in the Baltic Sea with increasing fCO_2

K. J. Crawfurd[1], U. Riebesell[2] , C. P. D. Brussaard[1,3]

[1]{NIOZ Royal Netherlands Institute for Sea Research, Department of Marine Microbiology and Biogeochemistry, and Utrecht University, P.O. Box 59, 1790 AB Den Burg, Texel, The Netherlands}

[2]{GEOMAR Helmholtz Centre for Ocean Research Kiel, Biological Oceanography, Düsternbrooker Weg 20, 24105, Kiel, Germany}

[3]{Aquatic Microbiology, Institute for Biodiversity and Ecosystem Dynamics, University of Amsterdam, P.O. Box 94248, 1090 GE Amsterdam, The Netherlands}

Correspondence to: kate.crawfurd@gmail.com

Abstract:

Ocean acidification, due to dissolution of anthropogenically produced carbon dioxide is considered a major threat to marine ecosystems. We examined the effects of ocean acidification on the microbial community structure in the Gulf of Finland, Baltic Sea, during the, inorganic nitrogen and phosphorus depleted, summer. Using large volume *in situ* mesocosms to simulate present to future and far future scenarios, we observed distinct trends with increasing fCO_2 in each of the 6 groups of phytoplankton enumerated by flow cytometry (<20 µm cell diameter). Of these groups 2 picoeukaryotic groups increased in abundance whilst the other groups, including prokaryotic *Synechococcus* spp., decreased

with increasing fCO_2. Gross growth rates increased with increasing fCO_2 in the dominant picoeukaryote group sufficient to double their abundances whilst reduced losses allowed the other picoeukaryotes to flourish at higher fCO_2. Converting abundances to particulate organic carbon we saw a large shift in the partitioning of carbon between the size fractions which lasted throughout the experiment. The prokaryotes largely followed the algal biomass with responses to increasing fCO_2 reflecting the altered phytoplankton community dynamics. Similarly, higher viral abundances at higher fCO_2 seemed related to increased prokaryote biomass. Viral lysis and grazing were both important in controlling prokaryotic abundances. Overall our results point to a shift towards a more regenerative system with potentially increased productivity but reduced carbon export.

1 Introduction

Ocean acidification (OA) caused by anthropogenic carbon dioxide (CO_2) release and its subsequent dissolution in the oceans is considered one of the great threats that marine ecosystems face (Turley and Boot, 2010). Direct and indirect effects are predicted to have a large impact on these ecosystems (IPCC, 2007). Phytoplankton production has been found susceptible to OA, depending on the phytoplankton community composition (eg. Hein and Sand-Jensen, 1997; Tortell et al., 2002; Leonardos and Geider, 2005; Engel et al., 2007; Feng et al., 2009). Calcification of coccolithophores, which influence sedimentation via calcium carbonate ballasting, is generally reduced (Meyer and Riebesell, 2015). Diatoms, important for organic matter burial, have been found to benefit in some cases (Feng et al., 2009) but not in others (Tortell et al., 2002). Certain cyanobacteria, including diazotrophs, have been seen to benefit from elevated CO_2 concentrations (Qiu and Gao, 2002; Barcelos e Ramos et al., 2007; Hutchins, 2007). Direct CO_2 effects are also reported for small-sized photoautotrophic eukaryotes (Engel et al., 2007; Meakin and Wyman, 2011; Brussaard et al., 2013).

Marine phytoplankton are responsible for approximately half of global primary production (Field et al., 1998), whereby shelf sea communities contribute 15-30% of this (Kulinski and Pempkowiak,

2011). Whilst environmental factors, such as temperature, light, nutrients and CO_2 concentration, regulate gross primary production bottom-up, loss factors (i.e., grazing, viral lysis and sedimentation) determine the fate of the carbon fixed by phytoplankton. Ingested carbon transfers to higher trophic levels, sinking of phytoplankton and faeces may lead to carbon storage in sediments, and viral lysis is a major driver of carbon release to dissolved and detrital organic matter (DOM; Wilhelm and Suttle, 1999; Brussaard et al., 2005; Lønborg et al., 2013). Through viral lysis the cell content of the host is released into the surrounding water and utilized by heterotrophic bacteria, thereby stimulating the microbial loop (Brussaard et al., 2008; Sheik et al., 2014). Bacteria may also be affected either directly by OA, or indirectly via changes in the quality or quantity of DOM (Weinbauer et al., 2011). Viral lysis has been found to be at least as important a loss factor as microzooplankton grazing for natural bacterio- and phytoplankton (Weinbauer, 2004; Baudoux et al., 2006; Evans and Brussaard, 2012; Mojica et al., 2016).

The effect of ocean acidification on the relative share of these key loss processes is, however, still understudied for most ecosystems, particularly for brackish coastal systems. Low salinity affects the pH buffering capacity due to low total alkalinity and is as such of interest for OA studies. Here we report on the temporal dynamics of microbes (phytoplankton, prokaryotes and viruses) under the influence of enhanced CO_2 concentrations and in relation to viral lysis and grazing control. Using large mesocosms at *in situ* light and temperature, the Baltic Sea pelagic ecosystem was exposed to a range of increasing CO_2 concentrations from ambient to future and far-future concentrations. This study was performed during summer in the Gulf of Finland near Tvärminne, with salinity around 5.7 and low dissolved inorganic nitrogen and phosphorus concentrations. During the 43 day long experiment the smallest picoeukaryotic phytoplankton especially showed distinct responses to the treatment conditions.

2 Materials and Methods

2.1 Study site and experimental set-up

The study was conducted in the Tvärminne Storfjärden (59° 51.5' N, 23° 15.5' E) between 14 June and 7 August, 2012. Nine mesocosms each enclosing ~ 55 m^3 of water with a depth of 17 m were moored in a square arrangement within the archipelago. For details on the experimental set-up, carbonate chemistry dynamics and nutrient concentrations throughout the experiment we refer to the general overview paper by Paul et al. (2015, this issue). After deployment the mesocosms were kept open for 5 days with 3 mm mesh screening over the top and bottom openings before being closed at the bottom and pulled above the sea surface at the top. Photosynthetically active radiation (PAR) transparent plastic hoods (open on the side) prevented rain and bird droppings from entering the mesocosms. Six mesocosms were sampled for the current study, unfortunately three were lost due to leakage. Initial fugacity of CO_2 (fCO_2) was 240 µatm. The mean fCO_2 during the experiment, i.e. days 1-43, for the individual mesocosms was as follows: M1, 365 µatm; M3, 1007 µatm; M5, 368 µatm; M6, 821 µatm; M7, 497 µatm; M8, 1231 µatm . Throughout this study we refer to fCO_2 which takes into account the non-ideal behavior of CO_2 gas and is the standard measurement required for gas exchange calculations (Pfeil et al., 2013).

For fCO_2 manipulations, natural seawater was saturated with CO_2 and then injected evenly throughout the whole depth of the mesocosms in four steps between days 0 to 3 until target fCO_2 was reached. On day 15 a further fCO_2 addition was made to the top 7 m of mesocosms 3, 6, and 8 to replace CO_2 lost due to outgassing. The remaining mesocosms received similar treatment without CO_2. Initial nutrient concentrations, i.e. nitrate, phosphate, silicate and ammonium, were 0.05 µmol L^{-1}, 0.15 µmol L^{-1}, 6.2 µmol L^{-1} and 0.2 µmol L^{-1}, respectively, and stayed low for the duration of the experiment (Paul et al., 2015, this issue). Salinity was around 5.7, temperature was initially ≈8°C and rose to ≈15°C on day 15 before falling to ≈8°C again.

Collective sampling was performed daily in the morning, using an integrated water sampler, from the top (0-10 m) and from the whole water column (0-17 m) of all mesocosms and the surrounding water. Subsamples were obtained for enumeration of phytoplankton, prokaryotes and viruses. Samples for viral lysis and grazing were taken from 5 m depth using a gentle vacuum-driven pump system. Samples were protected against daylight and warming by thick black plastic bags containing wet ice. In the laboratory the samples were processed at *in situ* temperature and dimmed light. As viral lysis and grazing rates were determined from samples taken from 5 m depth, samples for microbial abundances reported were taken from the top 10 m integrated samples. For abundances from 0-17 m and the surrounding water see Supplementary data (Table S1 and Fig.S1).

The experiment has been divided into 4 phases based on major physical and biological changes occurring (Paul et al., 2015). Phase 0 before CO_2 addition (days -5 to 0), phase I (days 1-16), phase II (days 17-22) and phase III (days 23-43). Throughout this study the data are presented using 3 colors (blue, grey and red), representing low (mesocosms M1 and M5) intermediate (M6 and M7) and high (M3 and M8) fCO_2 (Table 1).

2.2 Microbial abundances

Microbes were enumerated using a Becton Dickinson FACSCalibur flow cytometer (FCM) equipped with a 488 nm argon laser. The photoautotrophic cells (<20 µm) were counted directly fresh and were discriminated by their autofluorescent pigments (Marie et al., 1999). The samples were held on wet ice in the dark until counting. Based on their chlorophyll red autofluorescence and the presence of phycoerythrin orange autofluorescence in combination with side scatter signal, the phytoplankton community could be divided into 6 clusters. Phytoplankton cell size of the different phytoplankton clusters was determined by gentle filtration through 25 mm diameter polycarbonate filters

(Whatman) with a range of pore sizes (12, 10, 8, 5, 3, 2, 1, and 0.8 µm) according to Veldhuis and Kraay (2004). Average cell sizes of the different phytoplankton groups were 1, 1, 3, 2.9, 5.2, and 8.8 µm diameter for the prokaryotic cyanobacteria *Synechococcus* spp. (SYN), picoeukaryotic phytoplankton I, II and III (Pico I-III), and nanoeukaryotic phytoplankton I, and II (Nano I, II), respectively. Pico III was discriminated from Pico II (comparable average cell size) by higher orange autofluorescence. Cyanobacterial species *Prochlorococcus* spp. were not observed during this experiment. Assuming the cells to be spherical and applying conversion factors of 237 fg C μm^{-3} (Worden et al., 2004) and 196.5 fg C μm^{-3} (Garrison et al., 2000) for pico- and nano-sized plankton, respectively, cellular carbon was calculated based on the average cell diameters. Net growth and loss rates of phytoplankton and heterotrophic prokaryotes were derived from exponential regression analysis of the cell abundances.

Abundances of prokaryotes and viruses were determined from 0.5 % glutaraldehyde fixed, flash frozen (-80°C) samples according to Marie et al. (1999) and Brussaard (2004), respectively. The prokaryotes include bacteria, archaea and unicellular cyanobacteria, the latter accounting for maximal 10% of the total abundance. In the surface waters of the Baltic Sea most prokaryotes are heterotrophs (Riemann et al., 2008).

Briefly, thawed samples were diluted with sterile autoclaved Tris-EDTA buffer (10mM Tris-HCl and 1mM EDTA, pH 8.2) and stained with the green fluorescent nucleic acid-specific dye SYBR-Green I (Invitrogen Inc.) to a final concentration of the commercial stock of 1×10^{-4} (for prokaryotes) or 0.5×10^{-4} (for viruses). Virus samples were stained at 80°C for 10 min and then allowed to cool for 5 min at room temperature in the dark. Prokaryotes were stained for 15 min at room temperature in the dark (Brussaard, 2004 with adaptation according to Mojica et al., 2014). Prokaryotes and viruses were discriminated in bivariate scatter plots of green fluorescence versus side scatter. Final counts were corrected for blanks prepared and analysed like the samples. Two groups of prokaryotes were

identified as low (LDNA) and high DNA (HDNA) fluorescence prokaryotes by their stained nucleic acid fluorescence. Four viral groups (V1–4) were distinguished, whereby V1-V3 showed increasing green nucleic acid fluorescence (with similar side scatter signatures) and cluster V4 had similar green fluorescence to V3 but had higher side scatter similar to a virus infecting nano-eukaryotic algae (Baudoux and Brussaard, 2005).

2.3 Viral lysis and grazing

Microzooplankton grazing and viral lysis of phytoplankton was determined using the modified dilution method (Mojica et al., 2016). All seawater handling was performed at *in situ* temperature under dim light conditions using nitrile gloves. Briefly, one of two series of dilutions of 20, 40, 70 and 100% whole seawater (200 µm mesh sieved), was gently mixed with 0.45 µm filtered seawater (i.e. microzooplankton grazers removed) and the second series with 30 KDa filtered seawater (i.e. grazers and viruses removed). The dilution reduced the grazing and lysis pressure in a serial manner and regression analysis allowed loss rates (slope) and gross phytoplankton growth rates, in the absence of grazing and lysis (intercept y axis 30 kDa series), to be determined. The 0.45 µm filtrate was produced by gravity filtration of, 200 µm mesh sieved, seawater through a 0.45 µm Sartopore capsule filter. The 30 KDa ultrafiltrate was produced by tangential flow filtration of, 200 µm pre-sieved, seawater using a 30 kDa Vivaflow 200 PES membrane tangential flow cartridge (Vivascience). Incubations were set up in triplicate in clear 1.2 L polycarbonate bottles. They were suspended close to the mesocosms in small cages at 5 m depth for 24 hours. Subsamples were taken at 0 and 24 h, and phytoplankton abundances of the grazing series (0.45 µm diluent) were enumerated fresh by FCM. Due to time constraint, samples from the 30 kDa series were fixed to a 1% final concentration with formaldehyde:hexamine solution (18% v/v:10% w/v), stored for 30 min at 4°C, flash frozen in liquid nitrogen and stored at –80°C until flow cytometry analysis. The effects of fixation were tested periodically by running duplicate series of fresh and frozen samples. No differences in analysis

between fresh and frozen samples were observed. Incubation experiments were run with samples from mesocosm 1 (low fCO_2) and 3 (high fCO_2); due to the logistics of handling times it was not possible to do more. Experiments were performed until day 31. Occasionally the dilution assays displayed a positive slope rather than a negative slope for apparent growth rate versus fraction of natural water (thus not resulting in a reduction in mortality with dilution). Furthermore, very low phytoplankton abundances complicate proper analysis (and consequently results) due to the fact that the assay is based on a dilution series. Such assays were deemed failed. Further discussion of potential causes of positive regressions can be found in Kimmance and Brussaard (2010) and Stoecker et al. (2015).

Viral lysis of prokaryotes was determined by the method of Winget et al. (2005) adapted from the original method by Wilhelm et al. (2002). Here free viruses are removed from a sample of prokaryotes, samples are then taken every 3 hours for 24 hours for virus enumeration. Any viruses in the samples must come from lysing bacteria and thus the rate of bacterial lysis can be estimated using an appropriate burst size. Briefly, free viruses were removed from a 300 ml sample of whole water by re-circulation over a 0.2 µm pore size polyether sulfone membrane (PES) tangential flow filter (Vivaflow 50, Vivascience) at a filtrate expulsion rate of 40 ml min^{-1}. A total of 900 ml of virus-free seawater, freshly produced by 30 kDa ultrafiltration using a PES membrane (Vivaflow 200, Vivascience) was added in three steps to wash away free viruses. Finally the sample was diluted back to the original 300 ml volume with virus-free seawater. The samples were aliquoted into six 50 ml polycarbonate tubes. Mytomycin C (Sigma-Aldrich) (final concentration, 1 µg ml^{-1}, maintained at 4°C), which induces lysogenic bacteria (Weinbauer and Suttle, 1996) was added to three of the six tubes for each mesocosm studied. A third series of incubations with 0.2 µm filtered samples was used as a control for viral loss (e.g. viruses adhering to the tube walls) and showed no significant loss of free viruses during the incubations. At the start of the experiment, 1 ml subsamples were immediately removed from each tube and fixed as previously described for viral and bacterial abundance. The samples were incubated at *in situ* temperature in the dark and 1 ml subsamples

were then taken after 3h, 6h, 9h, 12h and 24h. Viruses were later enumerated by the method of Brussaard (2004) to determine their rate of production over time. Virus production was determined from linear regression of viral abundance over time (time period used for regression analysis may vary between sampling days, depending on the temporal virus abundance dynamics). Although experiments were performed with mesocosms 1, 2, and 3 as low, mid and high fCO_2, mesocosm 2 was lost due to leakage. Due to logistical reasons we were only able to perform these assays until day 21.

To determine grazing rates on prokaryotes, fluorescently labeled bacteria (FLB) were prepared from cultured *Halomonas halodurans* labeled with 594,6-Dichlorotriazinyl Aminofluorescein (DTAF, 40 µg ml^{-1}) according to Sherr and Sherr (1993). Frozen ampoules containing prey (1% of total bacteria) were added to triplicate 1 L incubation bottles containing whole water gently passed through 200 µm mesh. Twenty milliliter samples were taken immediately (0 h) and the headspace was removed by gently squeezing the bottle so that no air bubble remained. The samples were fixed with 1% final concentration 0.2 µm filtered gluteraldehyde (EM-grade, 25%) and stained with 0.2 µm filtered (Acrodisc ®25mm Syringe filters, PALL Life Sciences) DAPI at a final concentration of 2 µg ml^{-1} (Sherr et al., 1993). Samples were incubated for 30 min at 4°C and stored in the dark. The 1 L bottles were incubated on a slow turning wheel (1 rpm) at *in situ* light and temperature conditions for 24 h. 24 h samples were then taken in the same manner as for 0 h. Samples were filtered onto 25 mm, 0.2 µm black polycarbonate filters (GE Healthcare life sciences), mounted on microscopic slides and stored at -20°C until analysis. FLBs present on a ≈0.75mm^2 area were counted using a Zeiss Axioplan 2 microscope. Grazing (µ d^{-1}) was measured according to

$$N_{T24} = N_{T0} * e^{-\mu t},$$

where N_{T24} and N_{T0} are the number of FLBs present at 24 h and 0 h, respectively.

2.4 Statistics

Microzooplankton grazing rates were estimated from the regression coefficient of the apparent growth rate versus fraction of natural seawater for the 0.45-µm series, with the combined rate of viral-induced lysis and microzooplankton grazing being estimated from a similar regression for the 30-kDa series (Baudoux et al., 2006; Kimmance and Brussaard, 2010). A significant difference between the two regression coefficients (as tested by analysis of covariance) indicated a significant viral lysis rate. Phytoplankton gross growth rate, in the absence of grazing and viral lysis, was derived from the y intercept of the 30-kDa series regression. Similarly significant differences between mesocosms M1 and M3 were determined by analysis of covariance of regression lines of the dilution series for the two mesocosms. Students T-tests were used to determine significant differences between mesocosms for other parameters.

3 Results

3.1 Phytoplankton population dynamics

Phytoplankton showed two main peaks in abundance, at the start of the experiment (day 4, phase I) and day 24 (phase II; Fig. 1a). At the end of phase I the high fCO_2 mesocosms displayed higher phytoplankton abundance than the present day (low) fCO_2, whereas the opposite was found for days 17-22. These trends were largely due to the prokaryotic cyanobacteria *Synechococcus* spp., making up on average 74% of total abundance. In contrast, the total eukaryotic phytoplankton showed a strong positive effect of fCO_2 (Fig. 1b), due to the response of Pico I and II. For all phytoplankton groups, except *Synechococcus* and Pico III, we found the abundances in the surrounding water (Table

S1) largely comparable to the temporal dynamics in the mesocosms, with only occasionally higher abundances for the nanoeukaryotic phytoplankton groups and lower abundances for Pico I and II (Table S1, Fig. S1). The surrounding waters were more similar to the low fCO_2 than the high fCO_2 mesocosms, demonstrating that the differences between the low and high fCO_2 mesocosms are the effect of the elevated fCO_2. Phytoplankton, prokaryotes and viral abundances in the 0-17m samples were generally lower but showed similar dynamics (Figs. S1 and S2).

3.1.1 *Synechococcus*

Synechococcus (SYN) showed an initial peak in abundance on day 4 (Fig. 2a), then abundances declined, most so for the low fCO_2 mesocosms from days 4-7. The net growth rate was strongly negatively correlated with fCO_2 (R^2=0.98, Fig. 2d). The loss measurements (only grazing, no viral lysis detected) confirmed that the total loss rate for the low fCO_2 mesocosm M1 was significantly higher than for the high fCO_2 mesocosm M3 on day 10 (0.56 vs 0.27 d^{-1}), whilst the gross growth rate did not differ significantly (Fig. 2b). Cell abundances increased again from day 12. In the low fCO_2 mesocosms this continued until the bloom at day 24, whilst the high CO_2 mesocosms peaked at day 15 and then dropped again before increasing from days 19-24. Despite the deviation in temporal dynamics between the treatments, SYN abundance peaked at day 24 in all mesocosms with around 4.5 x 10^5 cells ml^{-1} (Fig 2a) and was negatively correlated with fCO_2 (R^2=0.77). Total net production during this bloom was greater in the low fCO_2 mesocosms than in the high ones as initial abundances were lower (day 13) and peak abundances higher (day 24; Fig. 2a). This could be explained by a higher total loss rate for M3 than M1 on day 17 (0.33 vs 0.17). The following decline (days 24-28) seemed largely due to reduced gross growth rates (Fig. 2b). Thereafter the trend was not so clear until the end of the experiment.

3.1.2 Picoeukaryotes I

Pico I was numerically the second most dominant group of phytoplankton, 26% of total phytoplankton abundances on average in the high fCO_2 mesocosms and 21% in the low CO_2 mesocosms. This amounts to 15% of total POC at high fCO_2, 10% at low fCO_2 (mean of total POC). The initial increase (peak in abundance at day 5, Fig. 3a) of these small-sized (mean cell diameter ≈1 µm, comparable to SYN) phytoplankton already showed a slight positive trend and strong correlation with fCO_2 for the net growth rate (Fig. 3d, R^2=0.95) and abundance (Fig. 3g, R^2=0.8). The higher loss rates (days 5 to 9; Fig. 3e) resulted in a decrease in abundance, which was stronger for the low fCO_2 mesocosms (as illustrated by M1) due to the significantly higher gross growth rates for the high fCO_2 mesocosm (represented by M3; Fig. 3b). The positive correlation of Pico I peak abundance with fCO_2 on day 13 (Fig. 3h, R^2=0.94) was lost upon another decline in abundance. Significantly higher losses at high fCO_2, a combination of grazing and lysis, resulted in a more dramatic crash at high fCO_2 and abundances becoming similar again around day 17 (Fig. 3a). Viral lysis was a significant loss factor compared to grazing, i.e. overall on average 45% and 70% of total losses in M1 and M3, respectively (Table S2). An extra addition of CO_2 was given to M3, M6 and M8 because their fCO_2 had approached that of the remaining mesocosms. This may have stimulated the gross growth in M3 for a longer period in the high fCO_2 mesocosms as compared to M1 (day 19; Fig. 3b). Combined with higher losses at low fCO_2 a positive correlation of net growth rates with fCO_2 was seen (Fig. 3f, R^2=0.71), and almost 2-fold higher abundances at high fCO_2 on day 21 (Fig. 3a, i, R^2=0.84). Pico I was thus greatly stimulated by increased fCO_2, from day 3 throughout the experiment. Standing stock of Pico I remained higher at high fCO_2 for the further duration of the experiment (Fig. 3a), with gross growth matched by total losses (Fig.3b). Surprisingly the higher abundances did not stimulate higher losses during this period, grazing rates were very low in both M1 and M3, and viral lysis was totally responsible for losses on day 31 in both mesocosms (Table S2).

3.1.3 Picoeukaryotes II

A group of larger picoeukaryotes, Pico II (mean diameter of 3 µm) bloomed exactly during the period Pico I was low in standing stock (days 13-21, Fig. 4a) and the peak abundance (day 17) correlated positively with fCO_2 (Fig. 4d). Relatively high total losses of 0.46 and 0.58 d^{-1} in the low and high fCO_2 mesocosms, respectively (average days 6-13) accompanied the high gross growth rates (0.69 and 0.72 d^{-1}) for the same period (Fig. 4b). These indicate high turnover and explain the slow rate of increase in cell abundance until day 13 (Fig. 4a). During the bloom period of Pico II, losses were smaller than the gross growth rate, more so it seems for M3 than M1 (Fig. 4b). Resultant net growth rates correlated with fCO_2 (Fig. 4d, R^2=0.82) with peak abundances 1.4 fold higher at high fCO_2 (Fig. 4a). Higher losses then contributed to the faster decline in abundances at high fCO_2. Phase III was a period of low turnover for Pico II with low gross growth and loss rates resulting in quite stable cell abundances, still higher at high fCO_2, until day 29 after which they declined in all mesocosms (Fig. 4a).

3.1.4 Picoeukaryotes III

Another group with around 2.9 µm cell diameter could be discriminated from Pico II by its higher orange autofluorescence, and as such may represent small-sized cryptophytes. This is just at the lower size range of small cryptophyte (Klaveness, 1989). This group (Pico III) had its highest abundances during phases II and III (days 17-43, Fig. 5a), with a distinct negative correlation to fCO_2 (Fig. 5e, R^2=0.91). Already directly upon the first CO_2 addition (days 0-4) the abundances declined for the high fCO_2 mesocosms (Fig. 5a) with net growth rates negatively correlated to fCO_2 (Fig. 5d, R^2=0.94). Gross growth rates were indeed significantly higher for M1 than M3 at days 1, 4 and 10 (Fig. 5b). Abundances of the Pico III group in the surrounding water followed the low fCO_2 mesocosms perfectly during this first period, indicating that the crash in the high fCO_2 mesocosms was indeed a direct (negative) effect of fCO_2 (Table S1). A similar response of Pico III abundance

halting in the high fCO_2 mesocosms and strongly increasing in the low fCO_2 mesocosms occurred directly after the additional fCO_2 purge (day 15). Losses were largely due to microzooplankton grazing. Unfortunately about half of the loss assays in the second half of the experiment failed (for unknown reasons), yet the successful assays suggest that losses were minor (Fig. 5b). There may also be larger cryptophytes present in the community, not counted by the flow cytometer because our data show Pico III most dominant in phase III whilst the specific pigment data shows a decline from phases 0 to III.

3.1.5 Nanoeukaryotes I

The nanoeukaryotes group Nano I consisted of cells with a mean diameter of 5.2 µm and were found with maximum abundances of 5.5 $x10^2$ ml^{-1} (Fig. 6a). After an initial peak at day 6, the lower fCO_2 mesocosms showed the highest numbers at day 17 (Fig. 6a). This seems initiated by 2.3-fold higher total loss rates for M3 than M1 on days 6 and 10 (Fig. 6b) in combination with 2-fold lower gross growth rates on day 10 (Fig. 6b). Ultimately, this led to net growth rates correlating negatively with fCO_2 for days 10-12 (Fig. 6d, R^2=0.83). Viral lysis occurred predominantly in the high fCO_2 mesocosm throughout the experiment with rates ranging from 0.13 to 0.7 day^{-1} (making up 16 to 98% of total losses; Table S2). A group of viruses which had a flow cytometric signal typical for viruses infecting nanoeukaryotes (V4) were identified but no obvious correlation was found with any of the phytoplankton groups. Lower total loss rates at days 13 and 17 in both mesocosms allowed a small increase in abundance, peaking on day 17 and negatively correlated to fCO_2 (Fig. 6e, R^2=0.67).

3.1.6 Nanoeukaryotes II

The temporal dynamics of Nano II were rather erratic (Fig. 7a). Nano II were the largest in size and may have been made up by different phytoplankton species, however due to their low numbers we were unable to discriminate separate groups. The peak in abundance at day 16 showed a negative

correlation to fCO_2 (Fig. 7e, R^2=0.61), and was the result of an overall reduced net growth rate with fCO_2 (Fig. 7d, R^2=0.56). The subsequent decline seems the result of reduced gross growth rate (to even zero) and increased loss rate (day 20; Fig. 7b).

3.1.7 Algal POC

The calculated mean algal POC shows that fCO_2 had a clear positive effect on the biomass of Pico I and II (Fig. 8a; p<0.0001). The effect became noticeable only a few days into the experiment and the mean Pico I and II POC concentrations in the high fCO_2 mesocosms stayed high for the entire duration of the experiment. At the same time the remaining algal groups showed reduced POC at enhanced fCO_2 (the sum of Pico III, and Nano I and II and *Synechococcus* spp.; Fig. 8b, p<0.01). Particularly Pico III showed a nearly instant and markedly negative response to increased fCO_2 concentration (Fig. S3a). This was a lasting effect as the strongest difference was found in the second half of the experiment. For Nano I and II the higher algal POC concentrations became only apparent from the end of phase I and during phase II (days 14-20; Fig. S3b). Due to its small cell size, the numerically dominant SYN accounted on average for 40% of total POC. Due to the exclusion of 3 mesocosms (see Material and Methods), the number of fCO_2 treatments is reduced to 6, which limits the statistical power of the results. Still, our data show that the responses of the different phytoplankton groups to ocean acidification were evident and consistent.

3.2 Prokaryote population dynamics

The prokaryotic temporal dynamics in the mesocosms resembled that in the outside waters (Fig. S2). In general prokaryote abundance in the mesocosms followed the total algal biomass, with an initial increase during the first days following the closure of the mesocosms (Fig. 9a). The increase was mainly due to the HDNA-prokaryotes (Fig. 9b). The total prokaryote abundance increased initially at a

net growth rate of 0.19 d^{-1}, and more specifically at 0.22 and 0.14 d^{-1} for the high and low DNA prokaryotes respectively (Fig. 9b and c). There was no significant difference in prokaryote abundance between the treatments at the first peak (day 4). However, grazing was significantly lower (0.3 d^{-1}) in high (M3) than in low (M1; 0.5 d^{-1}) CO_2 treatments, on both days 0 and 4, and viral lysis 3% higher at high CO_2 (Figs. 10b and c). The decline in prokaryote abundances from days 5 to 9 seemed due to declining phytoplankton biomass (Fig. 1a) and increasing viral lysis rates (12-16 % d^{-1} representing 39% of total losses in M1 and 37% in M3 on day 11, Fig. 10c). Viral lysis assays showed no evidence of lysogeny for the prokaryotic community during the experiment (all phases).

From days 10-15 prokaryote dynamics became clearly affected by fCO_2 with significantly higher abundances and net growth rates at higher fCO_2 (Fig. 9a). Both the HDNA and the LDNA-prokaryotes (peak abundance on day 13, Fig. 9b and c) showed significant correlation with fCO_2 (R^2= 0.92 and 0.79, respectively, total prokaryote R^2= 0.88, Fig. 10d). In the higher fCO_2 mesocosms the decline in prokaryote abundance following the peak at day 13 was largely the result of decreasing HDNA-prokaryote numbers (Fig. 9b). Grazing was indeed significantly higher in the high fCO_2 mesocosm M3 but the data for viral lysis were inconclusive due to a failed assay (for technical reasons) for M1 at day 14 (Fig. 10b and c). The significantly higher viral abundances, particularly due to the V3 group with highest green fluorescence, for the high fCO_2 mesocosms around that time (Figs. 11a and b) seem to indicate that viral lysis in the high fCO_2 mesocosms was higher.

During phase II prokaryote abundances increased steadily until day 24 (for both HDNA and LDNA), corresponding to increased algal biomass (Fig. 10e) and low grazing rates (0.1-0.2 d^{-1}; Fig. 10b). Although the overall higher prokaryote standing stock in the low fCO_2 mesocosms was due to enhanced growth around day 16 (Fig. 9a), the net growth rates were comparable after day 17. Moreover, the higher abundances were only found for the HDNA-prokaryotes (Fig. 9b and c). Viral

lysis rates were higher for the low fCO_2 mesocosms (Fig. 10c). The higher prokaryote abundances in the low fCO_2 mesocosms appear thus due to the lower grazing prior to the increase, i.e. at the end of phase I (day 14). Prokaryote abundance ultimately declined again during days 28-35, but less in M1 than in the other mesocosms (Fig. 9a). We unfortunately have no data of the prokaryote loss rates after day 25, however viral abundances increased at a steady rate of 2.2×10^6 d^{-1} (to a maximum of 0.9×10^8 ml^{-1} by day 39; Fig. 11a), implying that viral lysis was at least partly responsible for the decline in prokaryote abundance. There was no significant difference in viral abundances between the treatments during this period.

4 Discussion

At the start of the experiment the trophic conditions were typical for the Baltic Sea in summer, with depleted nutrient conditions, particularly nitrate (Paul et al., 2015), and a vertically stratified water column following the diatom-dominated spring bloom (Kuosa, 1991). The summer phytoplankton community was dominated by pico- and nano-sized phytoplankton, and these phytoplankton groups were of key importance during the experiment. Already at the start of the experiment more than 95% of the phytoplankton community was smaller than 20 µm cell diameter, and by day 5, 70% was smaller than 2 µm (Paul et al., 2015). The picoeukaryotic photoautotrophs Pico I and II showed a very strong fertilization effect with enhanced fCO_2, directly following the initial CO_2 additions until the end of the experiment. At the same time, the rest of the phytoplankton (Pico III, Nano I and II, and the prokaryote *Synechococcus* spp.) showed reduced abundances at higher fCO_2. These shifts in the size structure of the community could be explained by examining the gross growth rates in combination with the losses of the individual groups.

Overall, microbial temporal dynamics in the mesocosms were largely comparable to the surrounding water, with a few exceptions: i.e., phytoplankton Nano I and II occasionally showed much higher abundances whilst all the picoplankton abundances were lower in the surrounding waters. Higher abundances of nano-sized phytoplankton in the surrounding water were likely due to upwelling of cold, CO_2-rich deep water to the surface, bringing in inorganic nutrients, particularly silicate (Paul et al., 2015). Average temperatures in all the mesocosms and surrounding waters were similar, with the upwelling reducing the temperature from around 15 to 8°C during phase II. Along with reduced PAR (Paul et al., 2015) this generally reduced gross growth of the different phytoplankton groups however no synergistic effects with fCO_2 could be ascertained. The microbial population dynamics in the surrounding water more closely resembled those in the ambient fCO_2 mesocosms, and more importantly the differences were in contrast to the shifts in phytoplankton group dynamics in response to CO_2 enrichment. This implies that enhanced fCO_2 was indeed responsible for the changes seen.

4.1 Phase 0 (days -5 to 0), before CO_2 addition

In most experimental work nutrients have been added to stimulate phytoplankton growth, therefore little data exists for oligotrophic phytoplankton communities (Brussaard et al., 2013) with smaller sized algae typically dominating as they are better competitors for the growth-limiting nutrients (Raven, 1998; Veldhuis et al., 2005). Phase 0 shows the natural state of the ecosystem at the start of the experiment, with indeed a summer community dominated by picophytoplankton. Consistency in phytoplankton abundances across the mesocosms confirmed good replication and baseline data prior to CO_2 manipulation. The flow cytometric phytoplankton community was dominated by cyanobacteria *Synechococcus* spp. (SYN) and the smallest picoeukaryotes (Pico I; both around 1 µm). Picoeukaryotes are found in high numbers at this site throughout the year and *Synechococcus* only in summer when the temperatures are higher (Kuosa, 1991). Microscopic identification of

picoeukaryotes is extremely difficult and no species have been described for the region (Kuosa, 1991), however, pigment analyses suggest that Pico I and II are likely to be prasinophytes or other chlorophytes (Paul et al., 2015). Ideally, performing molecular analyses on the specific algal groups sorted by flow cytometry aids to identify group composition at the species level. Biomass of *Synechococcus* and Pico I increased steadily upon closure of the mesocosms due to high gross growth rates whilst the other groups dropped slightly in abundance. Our grazing rates of *Synechococcus* compare well to the average reported estimate of microzooplankton grazing on cyanobacteria in July in this region of 0.3 d^{-1} (range 0.18-0.53 d^{-1}, Kuosa, 1991). The net growth rates of the total prokaryotic community (0.19 d^{-1}) were also comparable to rates reported for this region (Kuosa, 1991). Because the losses (strongly dominated by grazing) were between 0.3-0.5 d^{-1}, their gross growth rates must have been around 0.5-0.7 d^{-1}.

4.2 Phase I (days 1-16)

According to Paul and coauthors (2015) Phase I was characterised by high productivity and high organic matter turnover. Indeed we saw all phytoplankton groups bloom and we measured relatively high losses by grazing and viral lysis for all groups, responsible for the referred high turnover of organic matter. The prokaryotes responded positively to the increased algal productivity and viral lysis. More specifically, during phase I Pico I benefitted directly and most from enhanced fCO_2 as demonstrated by their significantly ($p<0.05$) higher gross growth rates. Net growth rates of Pico II correlated positively with CO_2 enrichment, but somewhat later into phase I (days 12-17) due to reduced losses.

The stimulation of Pico I by elevated fCO_2 may be due to a stronger reliance on diffusive CO_2 entry compared to larger cells. Model simulations reveal that whilst near-cell CO_2/pH conditions are close to those of the bulk water for cells <5 µm in diameter, they diverge as cell diameters increase (Wolf-Gladrow and Riebesell, 1997; Flynn et al., 2012). This is due to the size-dependent thickness of the

diffusive boundary layer, which determines the diffusional transport across the boundary layer and to the cell surface (Wolf-Gladrow and Riebesell, 1997; Flynn et al., 2012). It is suggested that larger cells may be more able to cope with fCO_2 variability as their carbon acquisition is more geared towards dealing with low CO_2 concentrations in their diffusive boundary, e.g. by means of active carbon acquisition and bicarbonate utilization (Wolf-Gladrow and Riebesell, 1997; Flynn et al., 2012). However, as the Baltic Sea experiences particularly large seasonal fluctuations in pH and fCO_2 (Jansson et al., 2013) due to the low buffering capacity of the waters, phytoplankton here may be expected to have a high degree of physiological plasticity. Previous mesocosm studies reported enhanced abundances of the picoeukaryotic prasinophyte *Micromonas pusilla* at higher fCO_2 (Engel et al., 2007; Meakin and Wyman, 2011). Another summer mesocosm study in the Arctic revealed that even smaller picoeukaryotes, similar to Pico I in our study, showed a positive response to enhanced fCO_2 (Brussaard et al., 2013). Furthermore, Schaum et al. (2012) found that 16 ecotypes of *Ostreococcus tauri* (another prasinophyte similar in size to Pico I) increased in growth rate by 1.4-1.7 fold at 1,000 compared to 400 µatm pCO_2. All ecotypes increased their photosynthetic rates and those with most plasticity, most able to vary their photosynthetic rate in response to changes in fCO_2, were most likely to increase in frequency in the community. It is likely that the picoeukaryotes in our study, which show stimulation by fCO_2 are adapted to a highly variable carbonate system regime and are able to increase their photosynthetic rate when additional CO_2 is available. This ability could allow them to outcompete other phytoplankton (e.g., nanoeukaryotes during phase I) in an environment where nutrients are scarce.

Pico II population dynamics were, despite high gross growth rates, controlled by grazing at the start of the experiment, and only after a reduction in losses during phase II (more so for the high CO_2 mesocosms) could a bloom develop. For Nano I and Nano II the gross growth rates seemed to increase at higher fCO_2, but at the same time the losses also increased. However, differences in

growth and loss rates were not statistically significant and thus it stays difficult to underpin why these phytoplankton groups peaked to higher abundances at lower fCO_2 in phase I. Potentially released competition for nutrients towards the end of phase I (the numerically dominant Pico I and SYN had declined in abundance by then) aided the increase of the nanoeukaryotes.

In general, grazing was a substantial loss factor for all phytoplankton groups during this period and additionally Pico I and II, Nano I and II experienced noteworthy viral mediated mortality. The high grazing rates coincided with high abundances of the ciliate *Myrionecta rubra* at the start of the experiment (Lischka et al., 2015). After day 10 *M. rubra* abundances declined and correspondingly, abundances of most of the phytoplankton groups increased (Lischka et al., 2015). Occasionally grazing rates between the high fCO_2 (M3) and present-day low fCO_2 (M1) mesocosms differed significantly although no general trend could be observed. Very few studies have examined the effects of OA on microzooplankton grazing of phytoplankton (Suffrian et al., 2008; Rose et al., 2009; Brussaard et al., 2013). In neither of 2 mesocosm experiments did Suffrian et al. (2008) nor Brussaard (2013) see significant effects on grazing rates. However, in an on-board continuous culture experiment Rose et al. (2009) found that at elevated CO_2 concentrations higher prey abundances led to higher grazing rates. Similarly, Pico III in the current study during phase I was strongly negatively affected by CO_2 and showed congruently lower grazing rates at higher fCO_2. Nonetheless, this did not seem to hold for the high abundance groups SYN and Pico I, nor for Pico II with comparable abundances to Pico III. Alternatively the significantly reduced gross growth rates at high fCO_2 are the more likely cause for the clear differences in population dynamics between high and low fCO_2 treatments.

In contrast, higher gross growth rates alongside a predominance of viral lysis at high fCO_2 was seen in both Pico II and Nano I during phase I. Metabolically active cells were reported to be infected at higher rates and phytoplankton growing at higher growth rates produced more viral progeny, which could explain this observation (Bratbak et al., 1998; Weinbauer, 2004; Maat et al., 2014). Direct

effects of higher fCO_2 on viruses themselves are not expected as marine virus isolates were found to be quite stable (both particle and infectivity) over the range of pH obtained in the present study (Danovaro et al., 2011; Mojica and Brussaard, 2014). Besides lytic infection, there is the potential for a lysogenic viral life cycle, during which viral DNA is integrated in the host as a prophage (Weinbauer, 2004). We found, however, no evidence that the share of lysogeny compared to the lytic cycle was affected. In fact, the percentage lysogeny was found insignificant during the entire campaign. Mean viral abundances were higher under CO_2 enrichment towards the end of phase I, which is expected to be in response to increased phytoplankton and prokaryote biomass.

During Phase I the high turnover of phytoplankton biomass led to increasing growth of heterotrophic prokaryotes (Hornick et al., 2016). The enhanced net abundances (this study) were heavily grazed and additionally viral lysis became increasingly important (to 60% of total losses at the end of phase I). Bermúdez et al. (2016) reported highest biomass of protozoans around t15. This was predominantly the heterotrophic choanoflagellate *Calliacantha natans* (Hornick et al., 2016). *Calliacantha natans* feeds selectively only on particles <1 µm in diameter (Marchant and Scott, 1993) and therefore may graze on heterotrophic bacteria. During the second half of phase I significantly more prokaryotes were recorded in the high fCO_2 mesocosms, which was likely due to increased availability of dissolved organic carbon at high fCO_2 from higher rates of viral lysis of Pico II and Nano I initially (day 6) and Pico I and Nano II consecutively (day 10).

Assuming a cellular carbon conversion for phytoplankton cells of 237 fg C μm^{-3} (Worden et al., 2004) and 196.5 fg C μm^{-3} (Garrison et al., 2000) for pico- and nano-sized plankton, respectively, we calculated that viral lysis of phytoplankton between days 9 and 13 resulted in the release of 1.1 and 12.4 ng C ml^{-1} for M1 and M3, respectively. Similarly, assuming a bacterial growth efficiency of 30% and cellular carbon conversion of 7 fgC $cell^{-1}$ (Hornick et al., 2016), we estimated that the amount of organic carbon required to support bacterial growth during this period (taking into account the loss

of bacterial carbon due to grazing and viral lysis) was 0.7 ngC ml^{-1} in M1 and 11.0 ngC ml^{-1} in M3. Viral lysis of phytoplankton was thus an important source of organic carbon for the bacterial community and may have led to the observed differences between treatments.

4.3 Phase II (days 17-30)

Phase II displayed a second peak in total phytoplankton abundances related to increased picophytoplankton but reduced nanophytoplankton. Reduced microzooplankton grazing pressure on the picoeukaryotes and *Synechococcus* after day 17 allowed them to increase in abundance during Phase II. Microzooplankton abundances were reduced as compared to the start of the experiment (approximately an order of magnitude lower) and mesozooplankton increased (Lischka et al., 2015). Thus increased grazing of mesozooplankton on microzooplankton may have resulted in reduced grazing of, and proliferation of, picophytoplankton. .

Synechococcus bloomed during phase II, however with significantly lower abundances at higher fCO_2. So although Pico I benefitted from CO_2 enrichment, the similar sized *Synechococcus* did not. *Synechococcus* has shown diverse, strain-specific responses to CO_2 enrichment (Fu et al., 2007; Lu et al., 2006; Traving et al., 2014). As a prokaryote, *Synechococcus* has very different physiology from picoeukaryotes, needing extremely efficient CCMs due to the inefficiency of its Rubisco. Able to concentrate CO_2 to up to 1000-fold higher than the external medium (Badger and Andrews, 1982), they may attain maximal growth rates at the present-day CO_2 concentration (Low-Décarie et al., 2014).

The prokaryote abundance increased steadily during Phase II, again matching total phytoplankton dynamics. Following the initially higher prokaryote abundances at higher fCO_2 in Phase I, we found during phase II decreased abundances of HDNA-prokaryotes at high fCO_2. This fits with the reported reduced bacterial production (Hornick et al., 2015) and respiration measurements (Spilling et al., 2015) in these mesocosms during this time. The differences were due to an indirect effect on the prokaryotes of reduced phytoplankton growth by SYN, Pico III and Nano I leading to lower POC

concentrations at higher fCO_2. This was caused by reduced temperature and PAR (Paul et al., 2015). Indeed we saw only low grazing rates for this period and no significant differences in loss by either grazing or lysis, or in DOC (Paul et al., 2015). The steady increase in viral abundances from day 22 onwards indicates that viral lysis of the prokaryotes was substantial, which is confirmed by the halting of prokaryote growth, reduced bacterial production (Hornick et al., 2016) and ultimate decline in prokaryote abundance (this study). The estimated average viral burst size during phase III, obtained from the increase in total viral abundance and concomitant decline in bacterial abundances, was about 30 which is comparable to published values (Parada et al, 2006; Wommack and Colwell, 2000). Viral lysis rates of prokaryotes were measured until day 25 and indicated that on average 10-15% of the total population lysed per day (day 18-25). The final prokaryote abundance at the end of the experiment was in line with a continued lysis in that order of magnitude (corrected for reduced bacterial production; Hornick et al., 2016). Overall, the increased prokaryote activity during the first half of phase II, the relatively low phytoplankton activity during this phase and the (virally induced) mortality of the prokaryote community during the second half of phase II promotes the mineralization and increase in concentration of phosphate (particularly in the low fCO_2 mesocosms; Paul et al, 2015). To what extent elevated CO_2 concentration affects the reduction in P-release from biomass (Nausch et al., 2016), reduced respiration and bacterial production rates as seen in this study (Hornick et al., 2016; Spilling et al., 2016) needs to be explored still.

4.4 Phase III (days 31-43)

The positive growth response of the picoeukaryotes to earlier CO_2 enrichment was clearly reflected in the Chlorophyll a concentration, particulate organic carbon and phosphorus, and also in the dissolved organic carbon (DOC) pools in Phase III (Paul et al., 2015). This increase in DOC at high fCO_2 (Paul et al., 2015) may originate from viral lysis of prokaryotes and phytoplankton (Suttle 2005, Lønborg et al., 2013). We measured higher viral lysis rates for SYN, Pico II and Nano I, and similar

lysis rates but higher standing stock of Pico I at high fCO_2. Alternatively, increased fCO_2 coupled with low nutrient availability may have stimulated photosynthetic release of DOC and subsequent transparent exopolymer particles (TEP) formation (Engel, 2002; Borchard and Engel, 2012). TEP formation also results from sloppy feeding (Hasegawa et al., 2001; Møller, 2007) and viral lysis, and is thought to promote aggregation and sinking of particulate organic matter (Brussaard et al., 2008; Lønborg et al., 2013). Under the current conditions this would offset the reduced sedimentation associated with smaller cells (Sommer et al., 2002). However, no difference in sedimentation rates was reported between fCO_2 treatments for the current study (Paul et al., 2015). This may have been (partly) obscured by the negative correlation of diatoms, reported to have relatively higher sedimentation rates (Riebesell, 1989; Waite et al., 1997), with fCO_2 during phase III (Paul et al., 2015). At this stage it is hard to draw a final conclusion because at the same time there was a positive correlation with fCO_2 for larger-sized diatoms (>20 µm) (Paul et al., 2015). Because of the general urgency to know more about carbon sequestration, we recommend future studies on OA to focus not only on potential shifts in sedimentation due to changes in phytoplankton community composition, but also as a result of changes in phytoplankton size class in combination with the relative share of grazing and viral lysis (Brussaard et al., 2008).

5 Conclusions

Firstly, our data explain the majority of the phytoplankton dynamics in this mesocosm experiment as more than 90% of the Chl *a* was found in the <20 µm size fraction (Paul et al., 2015). Indeed these data allow us to examine the more detailed changes in community dynamics which are not obvious in the bulk measurements. Distinct shifts between more abundant pico-sized (0.2-3 µm) and nano-sized (3-20 µm) photoautotrophs were seen during the experiment which were also reflected in size-fractionated Chl a concentrations (Paul et al., 2015). Whilst other evident shifts in abundance and net growth rates between different picoeukaryote groups could only be revealed with the current

approach of using flow cytometry. Moreover, the complementary grazing and lysis loss rates (along with the gross growth rates) allowed for a more notable explanation of changes in the phytoplankton and prokaryote community.

Secondly, our study shows that CO_2 enrichment favors the net growth of the very small-sized (1 µm) picoeukaryotic phytoplankton. This positive response with fCO_2 is very specific, as neither *Synechococcus* spp., Pico III, nor the nanoeukaryotic phytoplankton groups displayed enhanced growth. Increasing atmosperic CO_2 leads to a number of further global changes, e.g. increasing sea surface temperatures (SST) which in turn strengthens vertical stratification and shoals mixed layer depth (Sarmiento et al., 1998; Toggweiler and Russell, 2008). Such changes in physicochemical conditions have been reported to favor small cells, largely because of reduced nutrient supply to the surface waters (Cermeño et al., 2008; Riebesell et al., 2009; Li et al., 2009; Craig et al., 2013; Mojica et al., 2016). The study by Mojica et al. (2016) shows that under such conditions the share of viral lysis vs grazing for a variety of phytoplankton groups increases, thereby promoting a more regenerative system.

The overall activity of prokaryotes is expected to be affected not only by viral lysis of phytoplankton and prokaryotes themselves, but also by higher SST. This results in increased enzyme activities, production and also respiration rates, polysaccharide release and TEP formation (Piontek et al., 2009; Wohlers et al., 2009; Borchard et al., 2011; Engel et al., 2011; Wohlers-Zöllner et al., 2011). Enhanced bacterial re-mineralization of organic matter could further increase the autotrophic production by the small-sized phytoplankton (Riebesell et al., 2009; Riebesell and Tortell, 2011; Engel et al., 2013). At the same time, through viral lysis and subsequent microbial respiration the biological pump is negatively affected by the production of atmospheric CO_2 (del Giorgio and Duarte, 2002). The evidence presented in the current study indicates that CO_2 enrichment favors small-sized picoeukaryotic phytoplankton, which is further strengthened by increased SST and enhanced vertical stratification. By and large these changes will tend to reduce carbon sequestration.

Author Contribution

Design and overall coordination of research by CB. Organization and performance of analyses in the field by KC. Data analysis by KC and CB. Design and coordination of the overall KOSMOS mesocosm project by UR. All authors contributed to the writing of the paper.

Acknowledgements

This project was funded through grants to C.B. by the Darwin project, the Netherlands Institute for Sea Research (NIOZ), and the EU project MESOAQUA (grant agreement number 228224). We thank the KOSMOS project organisers and team, in particular Andrea Ludwig, the staff of the Tvärminne Zoological Station and the diving team. We give special thanks to Anna Noordeloos, Kirsten Kooiman and Richard Doggen for their technical assistance during this campaign. We also gratefully acknowledge the captain and crew of R/V ALKOR for their work transporting, deploying and recovering the mesocosms. The collaborative mesocom campaign was funded by BMBF projects BIOACID II (FKZ 03F06550) and SOPRAN Phase II (FKZ 03F0611).

References

Amthor, J.: Respiration in a future, higher-CO_2 world, Plant, Cell & Environment, 14, 13-20, 1991.

Badger, M. R., Andrews, J., T., Whitney, S. M., Ludwig, M., Yellowlees, D. C., Leggat, W. and Price, D. G.: The diversity and coevolution of Rubisco, plastids, pyrenoids, and chloroplast-based CO_2-concentrating mechanisms in algae , Can. J. Bot., 76(6), 1052–1071, 1998.

Barcelos e Ramos, J., Biswas, H., Schulz, K. G., LaRoche, J. and Riebesell, U.: Effect of rising atmospheric carbon dioxide on the marine nitrogen fixer Trichodesmium, Global Biogeochem. Cycles, 21(2), doi:10.1029/2006GB002898, 2007.

Baudoux, A. C. and Brussaard, C. P. D.: Characterization of different viruses infecting the marine harmful algal bloom species Phaeocystis globosa, Virology, 341(1), 80–90, doi:10.1016/j.virol.2005.07.002, 2005.

Baudoux, A. C., Noordeloos, A. A. M., Veldhuis, M. J. W. and Brussaard, C. P. D.: Virally induced mortality of Phaeocystis globosa during two spring blooms in temperate coastal waters, Aquat. Microb. Ecol., 44(3), 207–217, doi:10.3354/ame044207, 2006.

Borchard, C. and Engel, A.: Organic matter exudation by *Emiliania huxleyi* under simulated future ocean conditions, Biogeosciences, 9(8), 3405–3423, doi:10.5194/bg-9-3405-2012, 2012.

Borchard, C., Borges, A. V., Händel, N. and Engel, A.: Biogeochemical response of *Emiliania huxleyi* (PML B92/11) to elevated CO_2 and temperature under phosphorous limitation: A chemostat study, J. Exp. Mar. Bio. Ecol., doi:10.1016/j.jembe.2011.10.004, 2011.

Bratbak G., Jacobsen A., Heldall M., Nagasaki K., Thingstad, F: Virus production in *Phaeocystis pouchetii* and its relation to host cell growth and nutrition, Aquat. Microb. Ecol., 16, 1-9, 1998.

Brussaard, C. P. D.: Optimization of Procedures for Counting Viruses by Flow Cytometry, Appl. Environ. Microbiol., 70(3), 1506–1513, doi:10.1128/AEM.70.3.1506-1513.2004, 2004.

Brussaard, C. P. D., Noordeloos, A. A. M., Sandaa, R. A., Heldal, M. and Bratbak, G.: Discovery of a dsRNA virus infecting the marine photosynthetic protist Micromonas pusilla, Virology, 319(2), 280–291, doi:10.1016/j.virol.2003.10.033, 2004.

Brussaard, C. P. D., Kuipers, B. and Veldhuis, M. J. W.: A mesocosm study of *Phaeocystis globosa* population dynamics: I. Regulatory role of viruses in bloom control, Harmful Algae, 4(5), 859–874, doi:10.1016/j.hal.2004.12.015, 2005.

Brussaard, C. P. D., Wilhelm, S. W., Thingstad, F., Weinbauer, M. G., Bratbak, G., Heldal, M., Kimmance, S. A., Middelboe, M., Nagasaki, K., Paul, J. H., Schroeder, D. C., Suttle, C. A., Vaqué, D. and Wommack, K. E.: Global-scale processes with a nanoscale drive: the role of marine viruses., ISME J., 2(6), 575–578, doi:10.1038/ismej.2008.31, 2008.

Brussaard, C. P. D., Noordeloos, A. A. M., Witte, H., Collenteur, M. C. J., Schulz, K., Ludwig, A. and Riebesell, U.: Arctic microbial community dynamics influenced by elevated CO_2 levels, Biogeosciences, doi:10.5194/bg-10-719-2013, 2013.

Cermeño, P., Dutkiewicz, S., Harris, R. P., Follows, M., Schofield, O. and Falkowski, P. G.: The role of nutricline depth in regulating the ocean carbon cycle., Proc. Natl. Acad. Sci. U. S. A., 105(51), 20344–20349, doi:10.1073/pnas.0811302106, 2008.

Craig, S. E., Thomas, H., Jones, C. T., Li, W. K. W., Greenan, B. J. W., Shadwick, E. H. and Burt, W. J.: Temperature and phytoplankton cell size regulate carbon uptake and carbon overconsumption in the ocean, Biogeosciences Discuss., 10(7), 11255–11282, doi:10.5194/bgd-10-11255-2013, 2013.

Danovaro, R., Corinaldesi, C., Dell'Anno, A., Fuhrman, J. A., Middelburg, J. J., Noble, R. T. and Suttle, C. A.: Marine viruses and global climate change. FEMS Microbiology Reviews, 35, 993–1034, 2011.

Dickinson, G. H., Matoo, O. B., Tourek, R. T., Sokolova, I. M. and Beniash, E.: Environmental salinity modulates the effects of elevated CO_2 levels on juvenile hard-shell clams, *Mercenaria mercenaria*., J. Exp. Biol., 216(Pt 14), 2607–18, doi:10.1242/jeb.082909, 2013.

Endres, S., Galgani, L., Riebesell, U., Schulz, K. G. and Engel, A.: Stimulated bacterial growth under elevated pCO_2: Results from an off-shore mesocosm study, PLoS One, 9(6), doi:10.1371/journal.pone.0099228, 2014.

Engel, A.: Direct relationship between CO_2 uptake and transparent exopolymer particles production in natural phytoplankton, J. Plankton Res., 24(1), 49–53, doi:10.1093/plankt/24.1.49, 2002.

Engel, A., Delille, B., Jacquet, S., Riebesell, U., Rochelle-Newall, E., Terbrüggen, A. and Zondervan, I.: Transparent exopolymer particles and dissolved organic carbon production by *Emiliania huxleyi* exposed to different CO_2 concentrations: a mesocosm experiment, Aquat. Microb. Ecol., 34, 93–104, 2004.

Engel, A., Schulz, K., Riebesell, U., Bellerby, R., Delille, B. and Schartau, M.: Effects of CO_2 on particle size distribution and phytoplankton abundance during a mesocosm bloom experiment (PeECE II), Biogeosciences Discuss., doi:10.5194/bgd-4-4101-2007, 2007.

Engel, A., Händel, N., Wohlers, J., Lunau, M., Grossart, H. P., Sommer, U. and Riebesell, U.: Effects of sea surface warming on the production and composition of dissolved organic matter during phytoplankton blooms: Results from a mesocosm study, J. Plankton Res., 33(3), 357–372, doi:10.1093/plankt/fbq122, 2011.

Engel, A., Borchard, C., Piontek, J., Schulz, K. G., Riebesell, U. and Bellerby, R.: CO_2 increases ^{14}C primary production in an Arctic plankton community, Biogeosciences, 10(3), 1291–1308, doi:10.5194/bg-10-1291-2013, 2013.

Evans, C., Archer, S.D., Jacquet, S. and Wilson, W.H. 2003. Direct estimates of the contribution of viral lysis and microzooplankton grazing to the decline of a *Micromonas* spp. population. Aquat. Microb. Ecol. 30: 207–219, doi:10.3354/ ame030207 2003.

Evans, C and Brussaard, C.P.D.: Regional Variation in Lytic and Lysogenic Viral Infection in the Southern Ocean and Its Contribution to Biogeochemical Cycling, Appl. Environ. Microbiol.,78(18), 6741-6748, 2012.

Feng, Y., Leblanc, K., Rose, J. M., Hare, C. E., Zhang, Y., Lee, P. A., Wilhelm, S. W., DiTullio, G. R., Rowe, J. M., Sun, J., Nemcek, N., Gueguen, C., Passow, U., Benner, I., Hutchins, D. A. and Brown, C.:

Effects of increased pCO_2 and temperature on the North Atlantic spring bloom. I. The phytoplankton community and biogeochemical response, , 388, 13–25, 2009.

Field, C. B., Behrenfeld, M. J., Randerson, J. T. and Falkowski, P.: Primary Production of the Biosphere: Integrating Terrestrial and Oceanic Components, Science 281(5374), 237–240, doi:10.1126/science.281.5374.237, 1998.

Flynn, K. J., Blackford, J. C., Baird, M. E., Raven, J. A., Clark, D. R., Beardall, J., Brownlee, C., Fabian, H. and Wheeler, G. L.: Letter. Changes in pH at the exterior surface of plankton with ocean acidification, Nat. Clim. Chang., 2(7), 510–513, doi:10.1038/nclimate1696, 2012.

Fu, F. X., Warner, M. E., Zhang, Y., Feng, Y. and Hutchins, D. A.: Effects of increased temperature and CO_2 on photosynthesis, growth, and elemental ratios in marine *Synechococcus* and *Prochlorococcus* (Cyanobacteria), J. Phycol., 43(3), 485–496, doi:10.1111/j.1529-8817.2007.00355.x, 2007.

Del Giorgio, P. A. and Duarte, C. M.: Respiration in the open ocean., Nature, 420(6914), 379–384, doi:10.1038/nature01165, 2002.

Grob, C., Hartmann, M., Zubkov, M. V. and Scanlan, D. J.: Invariable biomass-specific primary production of taxonomically discrete picoeukaryote groups across the Atlantic Ocean, Environ. Microbiol., 13(12), 3266–3274, doi:10.1111/j.1462-2920.2011.02586.x, 2011.

Gustafson Jr, D. E., Stoecker, D. K., Johnson, M. D., Heukelem, W. F., and Sneider, K.: Cryptophyte algae are robbed of their organelles by the marine ciliate Mesodinium rubrum, Nature, 405, 1049–1052, doi:10.1038/35016570, 2000.

Hasegawa, T., Koike, I., and Mukai.:Fate of food nitrogen in marine copepods. Mar. Ecol. Prog. Ser. 210, 167–174, 2001.

Hein, M. and Sand-Jensen, K.: CO_2 increases oceanic primary production, Nature, 388(6642), 526–527, 1997.

Hornick et al. Effect of ocean acidification on bacterial dynamics during a low productive late summer situation in the Baltic Sea Biogeosciences, (in prep.) 2016.

Hutchins, D. A.: CO_2 control of *Trichodesmium*, Limnol. Oceanogr., 52(4), 2007.

IPCC: IPCC Fourth Assessment Report: Climate Change 2007.

Jansson, A., Norkko, J. and Norkko, A.: Effects of Reduced pH on *Macoma balthica* Larvae from a System with Naturally Fluctuating pH-Dynamics, PLoS One, 8(6), doi:10.1371/journal.pone.0068198, 2013.

Kimmance, S. A. and Brussaard, C. P. D.: Estimation of viral-induced phytoplankton mortality using the, in Manual of Aquatic Viral Ecology, pp. 65–73., 2010.

Klaveness, D.: Biology and ecology of the Cryptophyceae: status and challenges., Biol Ocean., 6, 257–270, 1989.

Kulinski, K. and Pempkowiak, J.: The carbon budget of the Baltic Sea, Biogeosciences Discuss., 8, 4841–4869, 2011.

Kuosa, H.: Picoplanktonic algae in the northern Baltic Sea: seasonal dynamics and flagellate grazing, Mar. Ecol. Prog. Ser., 73(2-3), 269–276, doi:10.3354/meps073269, 1991.

Kuosa, H. and Kivi, K.: Bacteria and heterotrophic flagellates in the pelagic carbon cycle in the northern Baltic Sea, Mar. Ecol. Prog. Ser., 53(1975), 93–100, doi:10.3354/meps053093, 1989.

Landry, M. R. and Hassett, R. P.: Estimating the grazing impact of marine micro-zooplankton, Mar. Biol., 67(3), 283–288, doi:10.1007/BF00397668, 1982.

Larsen, J. B., Larsen, A., Thyrhaug, R., Bratbak, G. and Sandaa, R. A.: Response of marine viral populations to a nutrient induced phytoplankton bloom at different pCO_2 levels, Biogeosciences, 5, 523–533, doi:10.5194/bg-5-523-2008, 2008.

Lee, S. and Fuhrman, J.A., Relationships between Biovolume and Biomass of Naturally Derived Marine Bacterioplankton, Appl. Environ. Microbiol. 53(6), 1298-1303, 1987

Leonardos, N. and Geider, R. J.: Elevated atmospheric carbon dioxide increases organic carbon fixation by Emiliania huxleyi (Haptophyta), under nutrient-limited high-light conditions, J. Phycol., 41(6), 1196–1203 [online] Available from: http://dx.doi.org/10.1111/j.1529-8817.2005.00152.x, 2005.

Li, W. K. W., McLaughlin, F. A., Lovejoy, C. and Carmack, E. C.: Smallest algae thrive as the Arctic Ocean freshens., Science, doi:10.1126/science.1179798, 2009.

Lischka, S., Bach, L.T., Schulz, K.G., and Riebesell, U.: Micro- and mesozooplankton community response to increasing levels of fCO_2 in the Baltic Sea: insights from a large-scale mesocosm experiment, Biogeosciences, 2015

Lønborg, C., Middelboe, M. and Brussaard, C. P. D.: Viral lysis of *Micromonas pusilla*: Impacts on dissolved organic matter production and composition, Biogeochemistry, 116(1-3), 231–240, doi:10.1007/s10533-013-9853-1, 2013.

Low-Décarie, E., Fussmann, G. F. and Bell, G.: Aquatic primary production in a high-CO_2 world, Trends Ecol. Evol., 29(4), 223–232, doi:10.1016/j.tree.2014.02.006, 2014.

Lu, Z., Jiao, N. and Zhang, H.: Physiological changes in marine picocyanobacterial *Synechococcus* strains exposed to elevated CO_2 partial pressure, Mar. Biol. Res., 2(6), 424–430, doi:10.1080/17451000601055419, 2006.

Maat, D. S., Crawfurd, K. J., Timmermans, K. R. and Brussaard, C. P. D.: Elevated CO_2 and phosphate limitation favor *Micromonas pusilla* through stimulated growth and reduced viral impact, Appl. Environ. Microbiol., 80(10), 3119–3127, 2014.

Marchant, H.J. and Scott F.J: Uptake of sub-micrometre particles and dissolved organic material by Antarctic choanoflagellates, Mar. Ecol. Prog. Ser., 92, 59-64, 1993.

Marie, D., Brussaard, C. P. D., Thyrhaug, R., Bratbak, G. and Vaulot, D.: Enumeration of marine viruses in culture and natural samples by flow cytometry, Appl. Environ. Microbiol., 65(1), 45–52, 1999.

Meakin, N. G. and Wyman, M.: Rapid shifts in picoeukaryote community structure in response to ocean acidification., ISME J., doi:10.1038/ismej.2011.18, 2011.

Merkouriadi, I. and Leppäranta, M.: Long-term analysis of hydrography and sea-ice data in Tvärminne, Gulf of Finland, Baltic Sea, Clim. Change, 124(4), 849–859, doi:10.1007/s10584-014-1130-3, 2014.

Meyer, J. and Riebesell, U.: Reviews and Syntheses: Responses of coccolithophores to ocean acidification: a meta-analysis, Biogeosciences, 12(6), 1671–1682, doi:10.5194/bg-12-1671-2015, 2015.

Middelboe, M. and Lyck, P. G.: Regeneration of dissolved organic matter by viral lysis in marine microbial communities, Aquat. Microb. Ecol., 27(2), 187–194, doi:10.3354/ame027187, 2002.

Mojica, K. D. A. and Brussaard, C. P. D.: Factors affecting virus dynamics and microbial host–virus interactions in marine environments, FEMS Microbiol. Ecol., 89(3), 495–515, doi:10.1111/1574-6941.12343, 2014.

Mojica, K. D. A., Evans, C. and Brussaard, C. P. D.: Flow cytometric enumeration of marine viral populations at low abundances, Aquat. Microb. Ecol., 71(3), 203–209, doi:10.3354/ame01672, 2014.

Mojica, K. D. A., van de Poll, W. H., Kehoe, M., Huisman, J., Timmermans, K. R., Buma, A. G. J., van der Woerd, H. J., Hahn-Woernle, L., Dijkstra, H. A. and Brussaard, C. P. D.: Phytoplankton community structure in relation to vertical stratification along a north-south gradient in the Northeast Atlantic Ocean, Limnol. Oceanogr., 60(5), 1498–1521, doi:10.1002/lno.10113, 2015.

Mojica, K. D. A., Huisman, J., Wilhelm, S. W. and Brussaard, C. P. D.: Latitudinal variation in virus-induced mortality of phytoplankton across the North Atlantic Ocean, ISME J [online] Available from: http://dx.doi.org/10.1038/ismej.2015.130, 2016.

Møller Eva Friis: Production of dissolved organic carbon by sloppy feeding in the copepods Acartia tonsa, Centropages typicus, and Temora longicornis, Limnol. Oceanog.,, 52(1), 79-84 doi: 10.4319/lo.2007.52.1.0079, 2007.

Nausch, M., Bach, L., Czerny, J., Godstein, J., Grossart, H.-P., Hellemann, D., Hornick, T., Achterberg, E., Schulz, K.G and Riebesell, U.: Effects of CO_2 perturbation on phosphorus pool sizes and uptake in a mesocosm experiment during a low productive summer season in the northern Baltic Sea, Biogeosciences Discuss., 12, 17543-17593, doi:10.5194/bgd-12-17543-2015, 2015.

Parada, V., Herndl, G. and Weinbauer, M. :Viral burst size of heterotrophic prokaryotes in aquatic systems. J. Mar. Biol. Assoc. U. K., 86, 613-621. doi:10.1017/S002531540601352X, 2006.

Paul, A. J., Bach, L. T., Boxhammer, T., Czerny, J., Hellemann, D., Trense, Y., Nausch, M., Sswat, M., Riebesell, U., Road, M., Lismore, E. and Way, E.: Effect of elevated CO_2 on organic matter pools and fluxes in a summer , post spring-bloom Baltic Sea plankton community,Biogeosciences , 1–60, 2015.

Paulino, A. I., Egge, J. K. and Larsen, A.: Effects of increased atmospheric CO_2 on small and intermediate sized osmotrophs during a nutrient induced phytoplankton bloom, Biogeosciences Discuss., 4(6), 4173–4195, doi:10.5194/bgd-4-4173-2007, 2007.

Pfeil, B., Olsen, A., Bakker, D. C. E., Hankin, S., Koyuk, H., Kozyr, A., Malczyk, J., Manke, A., Metzl, N., Sabine, C. L., Akl, J., Alin, S. R., Bates, N., Bellerby, R. G. J., Borges, A., Boutin, J., Brown, P. J., Cai, W. J., Chavez, F. P., Chen, A., Cosca, C., Fassbender, A. J., Feely, R. A., González-Dávila, M., Goyet, C., Hales, B., Hardman-Mountford, N., Heinze, C., Hood, M., Hoppema, M., Hunt, C. W., Hydes, D., Ishii, M., Johannessen, T., Jones, S. D., Key, R. M., Körtzinger, A., Landschützer, P., Lauvset, S. K., Lefèvre, N., Lenton, A., Lourantou, A., Merlivat, L., Midorikawa, T., Mintrop, L., Miyazaki, C., Murata, A., Nakadate, A., Nakano, Y., Nakaoka, S., Nojiri, Y., Omar, A. M., Padin, X. A., Park, G. H., Paterson, K., Perez, F. F., Pierrot, D., Poisson, A., Ríos, A. F., Santana-Casiano, J. M., Salisbury, J., Sarma, V. V. S. S., Puhe, J., and Ulrich, B.: Global climate change and human impacts on forest ecosystems: postglacial development, present situation and future trends in Central Europe, Springer Science & Business Media, 2012.

Piontek, J., Händel, N., Langer, G., Wohlers, J., Riebesell, U. and Engel, A.: Effects of rising temperature on the formation and microbial degradation of marine diatom aggregates, Aquat. Microb. Ecol., 54, 305–318, doi:10.3354/ame01273, 2009.

Qiu, B. and Gao, K.: Effects of CO_2 enrichment on the bloom-forming cyanobacterium *Microcystis aeruginosa* (Cyanophyceae): Physiological responses and relationships with the availability of dissolved inorganic carbon, J. Phycol., 38(4), 721–729, doi:10.1046/j.1529-8817.2002.01180.x, 2002.

Raven, J. A.: The twelfth Tansley Lecture. Small is beautiful: The picophytoplankton, Funct. Ecol., doi:10.1046/j.1365-2435.1998.00233.x, 1998.

Riebesell, U.:Sinking of diatoms Mar. Ecol. Prog. Ser., 54: 109-119, 1989

Riebesell, U. and Tortell, P. D.: Effects of ocean acidification on pelagic organisms and ecosystems BT - Ocean Acidification, in Ocean Acidification, pp. 99–121, OUP Oxford. [online] Available from: http://books.google.com/books?hl=en&lr=&id=8yjNFxkALjIC&oi=fnd&pg=PA99&dq=effects+of+ocean+acidification+on+pelagic+organisms&ots=NfuXHN4lZ_&sig=FAEmNm76r7VSMadLGjwQfFMidNM\npapers2://publication/uuid/BEF2E67A-2360-42F4-9276-478DCFBC4E42, 2011.

Riebesell, U., Körtzinger, A. and Oschlies, A.: Sensitivities of marine carbon fluxes to ocean change., Proc. Natl. Acad. Sci. U. S. A., 106(49), 20602–20609, doi:10.1073/pnas.0813291106, 2009.

Riemann, L., Leitet, C., Pommier, T., Simu, K., Holmfeldt, K., Larsson, U. and Hagström, Å.: The Native Bacterioplankton Community in the Central Baltic Sea Is Influenced by Freshwater Bacterial Species , Appl. Environ. Microbiol., 74(2), 503–515, doi:10.1128/AEM.01983-07, 2008.

Rose, J. M., Feng, Y., Gobler, C. J., Gutierrez, R., Harel, C. E., Leblancl, K. and Hutchins, D. A.: Effects of increased pCO2 and temperature on the North Atlantic spring bloom. II. Microzooplankton abundance and grazing, Mar. Ecol. Prog. Ser., 388, 27–40, doi:10.3354/meps08134, 2009.

Sarmiento, J.L, Hughes, T.M.C., Stouffer, R.J and Manabe, S.: Simulated response of the ocean carbon cycle to anthropogenic climate warming, Nature 393, 245–249, 1998.

Schaum, E., Rost, B., Millar, A. J. and Collins, S.: Variation in plastic responses of a globally distributed picoplankton species to ocean acidification, , doi:10.1038/NCLIMATE1774, 2012.

Schlitzer, R., Schneider, B., Schuster, U., Sieger, R., Skjelvan, I., Steinhoff, T., Suzuki, T., Takahashi, T., Tedesco, K., Telszewski, M., Thomas, H., Tilbrook, B., Tjiputra, J., Vandemark, D., Veness, T., Wanninkhof, R., Watson, A. J., Weiss, R., Wong, C. S. and Yoshikawa-Inoue, H.: A uniform, quality controlled Surface Ocean CO_2 Atlas (SOCAT), Earth Syst. Sci. Data, 5(1), 125–143, doi:10.5194/essd-5-125-2013, 2013.

Sheik, A. R., Brussaard, C. P. D., Lavik, G., Lam, P., Musat, N., Krupke, A., Littmann, S., Strous, M. and Kuypers, M. M. M.: Responses of the coastal bacterial community to viral infection of the algae Phaeocystis globosa, ISME J., 8(1), 212–25, doi:10.1038/ismej.2013.135, 2014.

Sherr, E.B., D.A. Caron, and B. F. Sherr.: Staining of heterotrophic protists for visualization via epifluorescence microscopy, in Current Methods in Aquatic Microbial Ecology, edited by and J. C. P. Kemp, B. Sherr, E. Sherr, pp. 213–228, Lewis Publ., N.Y., 1993.

Sommer, U., Stibor, H., Katechakis, A., Sommer, F. and Hansen, T.: Pelagic food web configurations at different levels of nutrient richness and their implications for the ratio fish production:primary production, Hydrobiologia, 484(1-3), 11–20, doi:10.1023/A:1021340601986, 2002.

Spilling, K., Paul, A.J., Virkkala, N., Hastings, T., Lischka, S., Stuhr, A., Bermudez, R., Czerny, J., Schulz, KG., Ludwig, A. and Riebesell, U.: Ocean acidification decreases plankton respiration: evidence from a mesocosm experiment , Biogeosciences, (in prep.)2016

Suffrian, K., Simonelli, P., Nejstgaard, J. C., Putzeys, S., Carotenuto, Y. and Antia, A. N.: Microzooplankton grazing and phytoplankton growth in marine mesocosms with increased CO_2 levels, Biogeosciences, 5, 1145–1156, 2008.

Suttle, C. A.: Viruses in the sea., Nature, 437(7057), 356–361, doi:10.1038/nature04160, 2005.

Toggweiler, J.R. and Russell, J.: Ocean circulation in a warming climate, Nature 451, 286–288, 2008.

Tortell, P. D., DiTullio, G. R., Sigman, D. M. and Morel, F. M. M.: CO_2 effects on taxonomic composition and nutrient utilization in an Equatorial Pacific phytoplankton assemblage, Mar. Ecol. Prog. Ser., 236, 37–43, 2002.

Traving, S. J., Clokie, M. R. J. and Middelboe, M.: Increased acidification has a profound effect on the interactions between the cyanobacterium Synechococcus sp. WH7803 and its viruses, FEMS Microbiol. Ecol., 87(1), 133–141, doi:10.1111/1574-6941.12199, 2014.

Turley, C. and Boot, K.: UNEP emerging issues: Environmental consequences of ocean acidification: A threat to food security, United Nations Environ. Program., 2010.

Veldhuis, M. J. W. and Kraay, G. W.: Phytoplankton in the subtropical Atlantic Ocean: Towards a better assessment of biomass and composition, Deep. Res. Part I Oceanogr. Res. Pap., 51(4), 507–530, doi:10.1016/j.dsr.2003.12.002, 2004.

Veldhuis, M. J. W., Timmermans, K. R., Croot, P. and Van Der Wagt, B.: Picophytoplankton; A comparative study of their biochemical composition and photosynthetic properties, J. Sea Res., 53(1-2 SPEC. ISS.), 7–24, doi:10.1016/j.seares.2004.01.006, 2005.

Waite, A, Fisher, A, Thompson, P., Harrison, P.: Sinking rate versus cell volume relationships illuminate sinking rate control mechanisms in marine diatoms Mar. Ecol. Prog. Ser.,157, 97-108, 1997

Waterbury JB , WatsonSW, V. & F.: Biological and ecological characterization of the marine unicellular cyanobacterium *Synechococcus*., in Photosynthetic Picoplankton, edited by E. Platt, T. and Li, W., pp. pp. 71–120., Can. Bull. Fish. Aquat. Sci. 214., 1986.

Weinbauer, M. G.: Ecology of prokaryotic viruses, FEMS Microbiol. Rev., 28(2), 127–181, doi:10.1016/j.femsre.2003.08.001, 2004.

Weinbauer, M. G. and Suttle, C. A.: Potential significance of lysogeny to bacteriophage production and bacterial mortality in coastal waters of the Gulf of Mexico, Appl. Environ. Microbiol., 62(12), 4374–4380, 1996.

Weinbauer, M. G., Mari, X. and Gattuso, J.-P.: Effect of ocean acidification on the diversity and activity of heterotrophic marine microorganisms, in Ocean acidification, pp. 83–98., 2011.

Wilhelm, S. W. and Suttle, C. A.: Viruses and Nutrient Cycles in the Sea aquatic food webs, Bioscience, 49(10), 781–788, doi:10.2307/1313569, 1999.

Wilhelm, S. W., Brigden, S. M. and Suttle, C. A.: A dilution technique for the direct measurement of viral production: A comparison in stratified and tidally mixed coastal waters, Microb. Ecol., 43(1), 168–173, doi:10.1007/s00248-001-1021-9, 2002.

Winget, D. M., Williamson, K. E., Helton, R. R. and Wommack, K. E.: Tangential flow diafiltration: An improved technique for estimation of virioplankton production, Aquat. Microb. Ecol., 41(3), 221–232, doi:10.3354/ame041221, 2005.

Wohlers, J., Engel, A., Zöllner, E., Breithaupt, P., Jürgens, K., Hoppe, H.-G., Sommer, U. and Riebesell, U.: Changes in biogenic carbon flow in response to sea surface warming., Proc. Natl. Acad. Sci. U. S. A., 106(17), 7067–7072, doi:10.1073/pnas.0812743106, 2009.

Wohlers-Zöllner, J., Breithaupt, P., Walther, K., Jürgens, K. and Riebesell, U.: Temperature and nutrient stoichiometry interactively modulate organic matter cycling in a pelagic algal-bacterial community, Limnol. Oceanogr., 56(2), 599–610, doi:10.4319/lo.2011.56.2.0599, 2011.

Wolf-Gladrow, D. and Riebesell, U.: Diffusion and reactions in the vicinity of plankton: A refined model for inorganic carbon transport, Mar. Chem., 59(1-2), 17–34, doi:10.1016/S0304-4203(97)00069-8, 1997.

Wommack, K.E. and Colwell, R.R.:Virioplankton: viruses in aquatic ecosystems. Microbiol. Mol. Biol. Rev. 64, 69–114, 2000.

Zondervan, I., Rost, B. and Riebesell, U.: Effect of CO_2 concentration on the PIC/POC ratio in the coccolithophore Emiliania huxleyi grown under light-limiting conditions and different daylengths, J. Exp. Mar. Bio. Ecol., 272(1), 55–70 [online] Available from: http://www.sciencedirect.com/science/article/B6T8F-45D8N98-3/2/28501cce2a3ebd671b67516eeb41dac9, 2002.

Table 1. fCO_2 concentrations (µatm) as an average for the duration of the experiment following CO_2 addition and specification of this CO_2 level as low, medium or high. *denotes mesocosms sampled for grazing and viral lysis assays

Mesocosm	***M1****	***M5***	***M7***	***M6***	***M3****	***M8***
CO_2 Level	***LOW***	***LOW***	***INTERMEDIATE***	***INTERMEDIATE***	***HIGH***	***HIGH***
Mean fCO_2 (µatm) days 1-43	***365***	***368***	***497***	***821***	***1007***	***1231***
Symbol						

Figure captions

Fig. 1. a) Temporal dynamics of depth-integrated upper layer (0.3–10 m) total phytoplankton and **b)** total eukaryotic phytoplankton, ie. all except the prokaryotic photoautotroph *Synechococcus* spp.. Lines indicate the start and end of phase II. The colours and symbols used in the legend are consistent throughout subsequent figures and, in parenthesis, is shown the mean fCO_2 across the duration of the experiment ie. days 1-43 .

Fig. 2. a) Temporal dynamics of depth-integrated upper layer (0.3–10 m) total prokaryotic phytoplankton, *Synechococcus* spp., whereby the lines indicate the different phases (I-III). **b)** Gross growth rates and total loss rates in mesocosms M1 and M3. Gross growth displayed as bars above the X- axis and total losses as bars below the X-axis. Significant differences between mesocosms are marked: p≤0.001***, p≤0.01**, p ≤0.05*,p ≤0.1$^{\cdot}$ **c)** Abundances for mesocosm M1 (low fCO_2, blue line) and mesocosm M3 (high CO_2, red line). **d)** Specific growth rates derived from exponential regression of the net SYN abundances, versus average fCO_2 for days 4-7.

Fig. 3. a) Temporal dynamics of depth-integrated upper layer (0.3–10 m) picophytoplankton I (Pico I). **b)** Gross growth rates and total loss rates in mesocosms M1 and M3. Gross growth displayed as bars above the X- axis and total losses as bars below the X-axis. Significant differences between mesocosms are marked: p≤0.001***, p≤0.01**, p ≤0.05*,p ≤0.1$^{\cdot}$ **c)** Abundances for mesocosm M1 (low fCO_2, blue line) and mesocosm M3 (high CO_2, red line). **d)** Specific growth rates derived from exponential regression of the net Pico I abundances, versus average fCO_2 for days 1-5; **e)** days 5-9; **f)** days 18–t21, a negative growth rate indicates cell loss. **g)** Phytoplankton cell abundance versus actual fCO_2 for Pico I on days 5; **h)** 13 **i)** 21.

Fig. 4. a) Temporal dynamics of depth-integrated upper layer (0.3–10 m) picoeukaryotic phytoplankton II (Pico II). **b)** Gross growth rates and total loss rates in mesocosms M1 and M3. Gross growth displayed as bars above the X- axis and total losses as bars below the X-axis. A rate of zero is displayed as a 0 in the colour of the mesocosm it relates to. Significant differences between mesocosms are marked: p≤0.001***, p≤0.01**, p ≤0.05*,p ≤0.1· **c)** Abundances for mesocosm M1 (control, blue line) and mesocosm M3 (high CO_2, red line). **d)** Specific growth rate determined from the net Pico II abundances, versus average fCO_2 for days 12-17. **e)** Phytoplankton cell abundance versus actual fCO_2 for Pico I on day 17.

Fig. 5. a) Temporal dynamics of depth-integrated upper layer (0.3–10 m) picoeukaryotic phytoplankton III (Pico III). **b)** Gross growth rates and total loss rates in mesocosms M1 and M3. Gross growth displayed as bars above the X- axis and total losses as bars below the X-axis. No data indicates a failed experiment and a rate of zero as a 0 in the colour of the mesocosm it relates to. Significant differences between mesocosms are marked: p≤0.001***, p≤0.01**, p ≤0.05*,p ≤0.1· **c)** Abundances for mesocosm M1 (low fCO_2, blue line) and mesocosm M3 (high CO_2, red line). **d)** Specific growth rate determined from the net Pico III abundances, versus average fCO_2 for days 1-2. **e)** Phytoplankton cell abundance versus actual fCO_2 for Pico I on day 24.

Fig. 6. a) Temporal dynamics of depth-integrated upper layer (0.3–10 m) nanoeukaryotic phytoplankton I (Nano I). **b)** Gross growth rates and total loss rates in mesocosms M1 and M3. Gross growth displayed as bars above the X- axis and total losses as bars below the X-axis. No data indicates

a failed experiment and a rate of zero as a 0 in the colour of the mesocosm it relates to. Significant differences between mesocosms are marked: p≤0.001***, p≤0.01**, p ≤0.05*,p ≤0.1˙ **c)** Abundances for mesocosm M1 (low fCO_2, blue line) and mesocosm M3 (high CO_2, red line). **d)** Specific growth rate determined from the net Nano I abundances, versus average fCO_2 for days 10-12, a negative growth rate indicates cell loss **e)** Phytoplankton cell abundance versus actual fCO_2 for Nano I on day 17.

Fig.7. a) Temporal dynamics of depth-integrated upper layer (0.3–10 m) nanoeukaryotic phytoplankton II (Nano II). **b)** Gross growth rates and total loss rates in mesocosms M1 and M3. Gross growth displayed as bars above the X- axis and total losses as bars below the X-axis. No data indicates a failed experiment and a rate of zero as a 0 in the colour of the mesocosm it relates to. Significant differences between mesocosms are marked: p≤0.001***, p≤0.01**, p ≤0.05*,p ≤0.1˙ **c)** Abundances for mesocosm M1 (low fCO_2, blue line) and mesocosm M3 (high CO_2, red line). **d)** Specific growth rate determined from the net Nano II abundances, versus average fCO_2 for days 6-17 (M1, days 6-16) **e)** Phytoplankton cell abundance versus actual fCO_2 for Nano II on day 17 (M1, day 16).

Fig.8. POC calculated from mean cell abundances applying conversion factors of 237 fg C μm^{-3} (Worden et al.2004) and 196.5 fg C μm^{-3} (Garrison et al. 2000) for pico- and nano-sized plankton respectively, cellular carbon was calculated based on the average cell diameters. **a)** Temporal dynamics of Pico I and II **b)** Temporal dynamics of POC for all other eukaryotic groups ie. Pico III, Nano I and II.

Fig.9. a) Temporal dynamics of depth-integrated upper layer (0.3–10 m) total heterotrophic prokaryotes (HP) **b)** High DNA fluorescence heterotrophic prokaryotes (HDNA-HP) **c)** Low DNA fluorescence heterotrophic prokaryotes (LDNA-HP) .

Fig.10. a) M1 (low fCO_2) and M3 (high CO_2) temporal dynamics of total heterotrophic prokaryotes (HP) abundances **b)** grazing rates (d^{-1}) (bars below the X-axis). Significant differences between mesocosms are marked: p≤0.001***, p≤0.01**, p ≤0.05*,p ≤0.1· **c)** Viral lysis as percentage of HP standing stock in mescocosm M1 (low fCO_2, blue) and M3 (high fCO_2, red) **d)** Total HP cell abundance versus actual fCO_2 on day 13. **e)** Mean prokaryote abundances in high (3,6,8) and low CO_2 mesocosms (1,5,7) vs total particulate organic carbon (POC) calculated from total cell abundances, ie. all groups measured by flow cytometry, for both series R^2=0.7.

Fig.11. a) Temporal dynamics of depth-integrated upper layer (0.3–10 m) total virus abundances, **b)** Virus group V3, discriminated by its higher green nucleic acid-specific fluorescence.

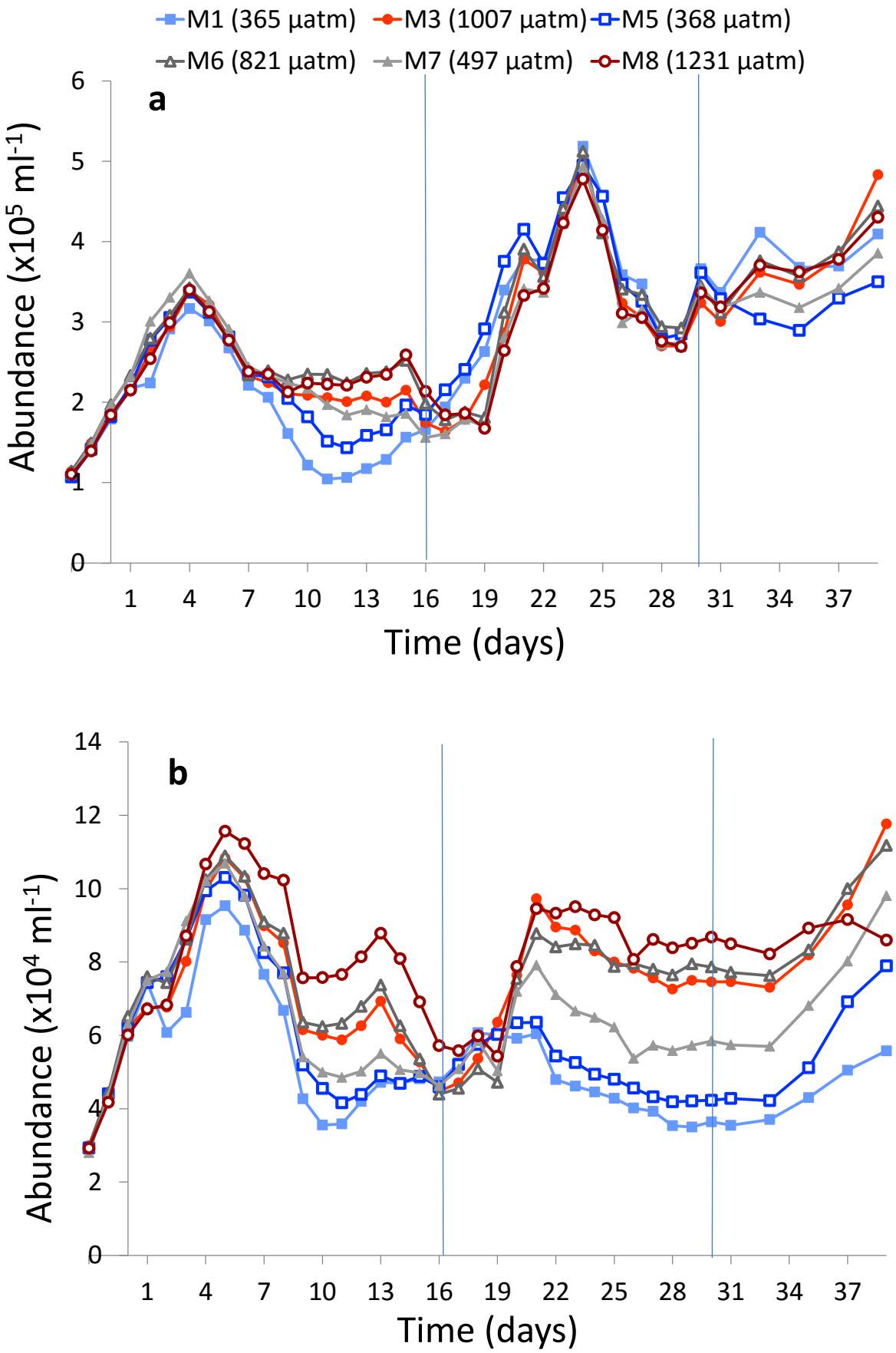
M1 (365 µatm)
M3 (1007 µatm)
M5 (368 µatm)
M6 (821 µatm)
M7 (497 µatm)
M8 (1231 µatm)
a
Abundance (x10^5 ml^{-1})
Time (days)
b
Abundance (x10^4 ml^{-1})
Time (days)

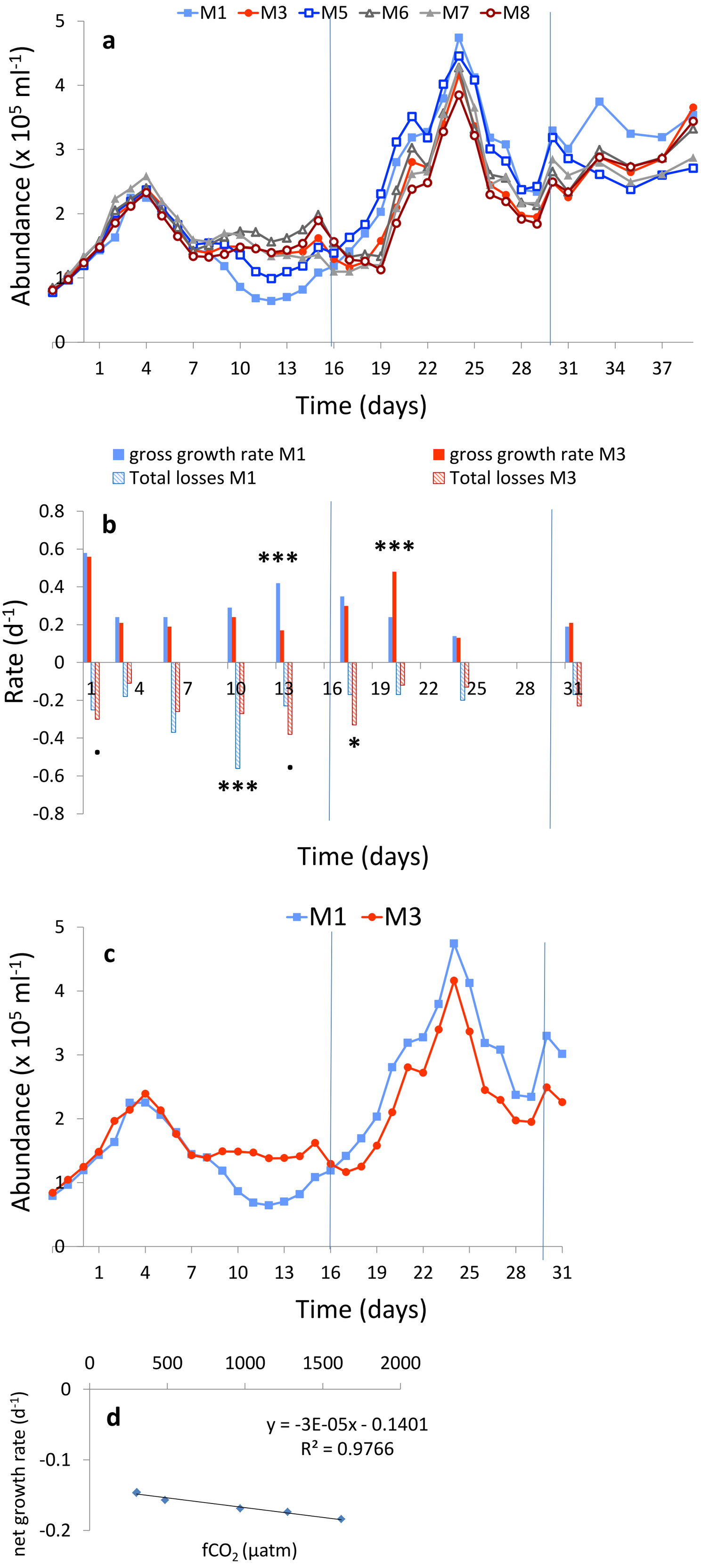
M1
M3
M5
M6
M7
M8
a
Abundance (x 10^5 ml^-1)
Time (days)
gross growth rate M1
gross growth rate M3
Total losses M1
Total losses M3
b
Rate (d^-1)
***
***
***
*
•
•
M1
M3
c
Abundance (x 10^5 ml^-1)
Time (days)
d
y = -3E-05x - 0.1401
R² = 0.9766
net growth rate (d^-1)
fCO2 (µatm)

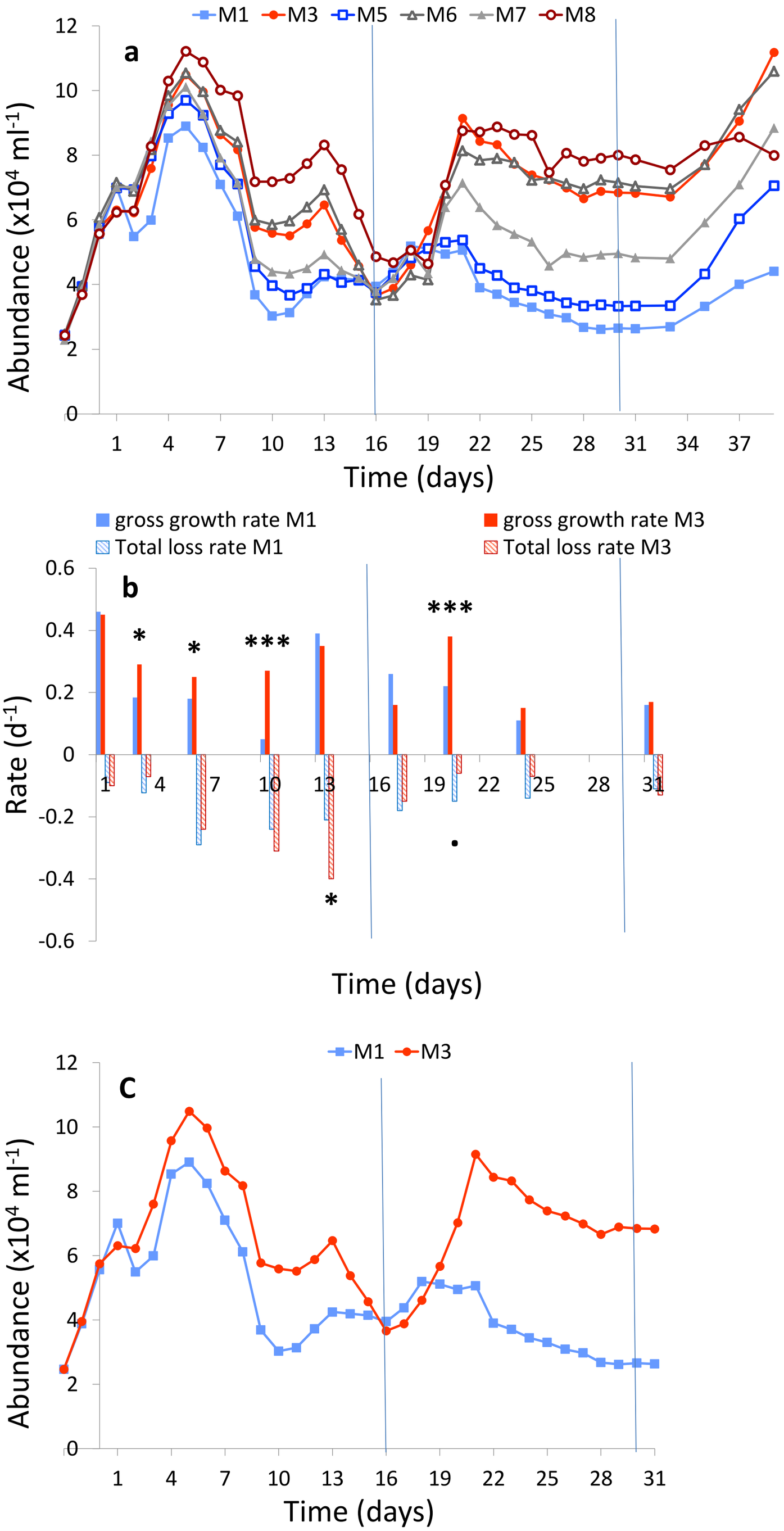
M1
M3
M5
M6
M7
M8
a
Abundance (x10⁴ ml⁻¹)
Time (days)
gross growth rate M1
gross growth rate M3
Total loss rate M1
Total loss rate M3
b
Rate (d⁻¹)
Time (days)
M1
M3
c
Abundance (x10⁴ ml⁻¹)
Time (days)

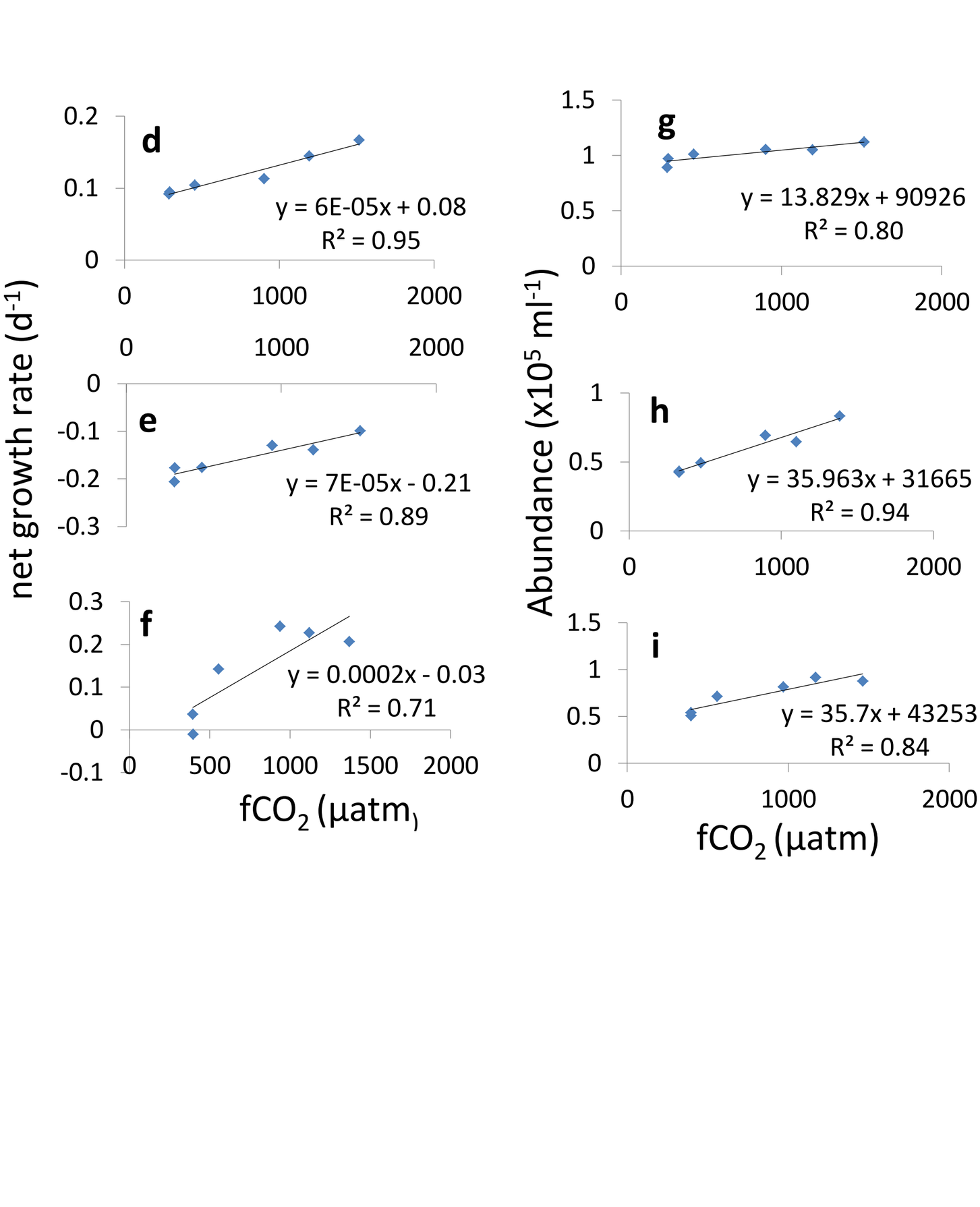
net growth rate (d-1)
Abundance (x105 ml-1)
d
y = 6E-05x + 0.08
R² = 0.95
e
y = 7E-05x - 0.21
R² = 0.89
f
y = 0.0002x - 0.03
R² = 0.71
fCO2 (µatm)
g
y = 13.829x + 90926
R² = 0.80
h
y = 35.963x + 31665
R² = 0.94
i
y = 35.7x + 43253
R² = 0.84
fCO2 (µatm)

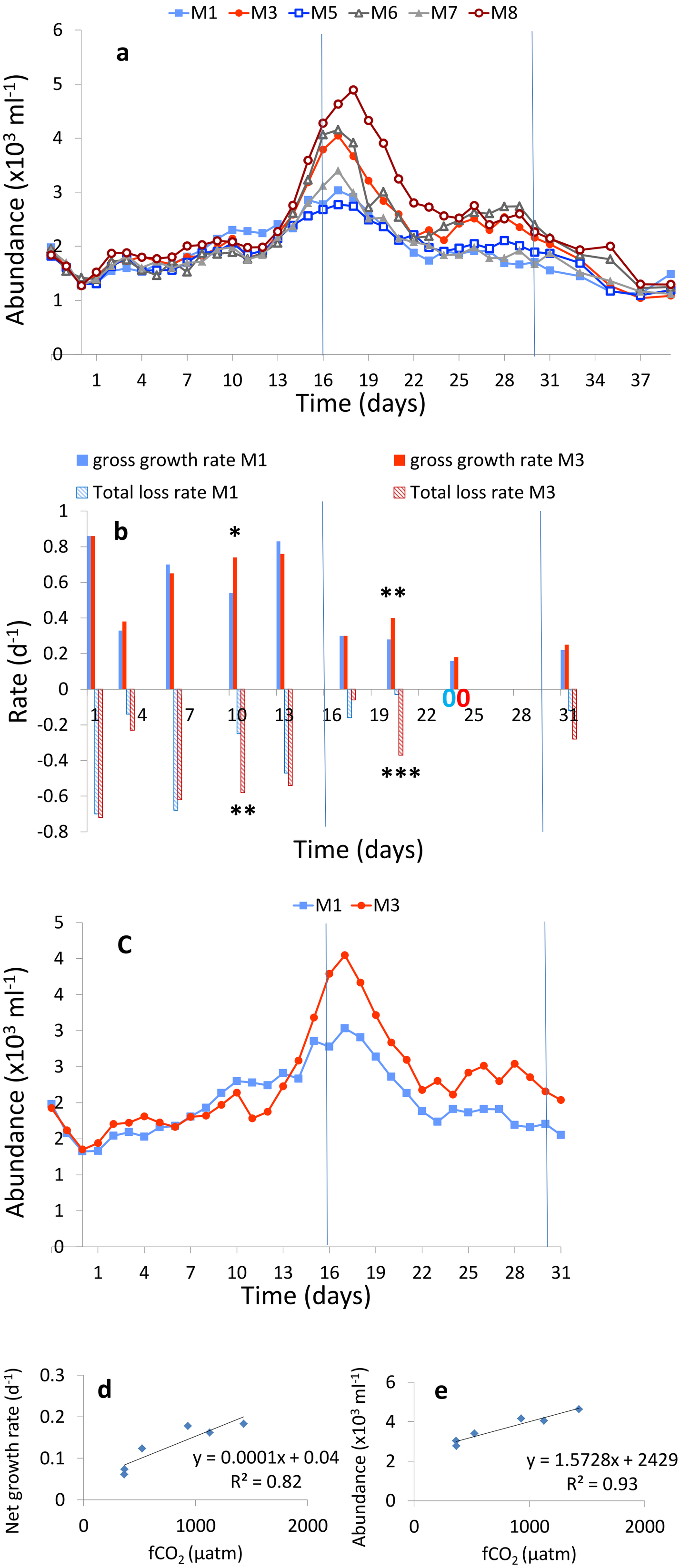
M1
M3
M5
M6
M7
M8
a
Abundance (x10³ ml⁻¹)
Time (days)
gross growth rate M1
gross growth rate M3
Total loss rate M1
Total loss rate M3
b
Rate (d⁻¹)
*
**
**
***
00
Time (days)
M1
M3
c
Abundance (x10³ ml⁻¹)
Time (days)
d
Net growth rate (d⁻¹)
y = 0.0001x + 0.04
R² = 0.82
fCO₂ (µatm)
e
Abundance (x10³ ml⁻¹)
y = 1.5728x + 2429
R² = 0.93
fCO₂ (µatm)

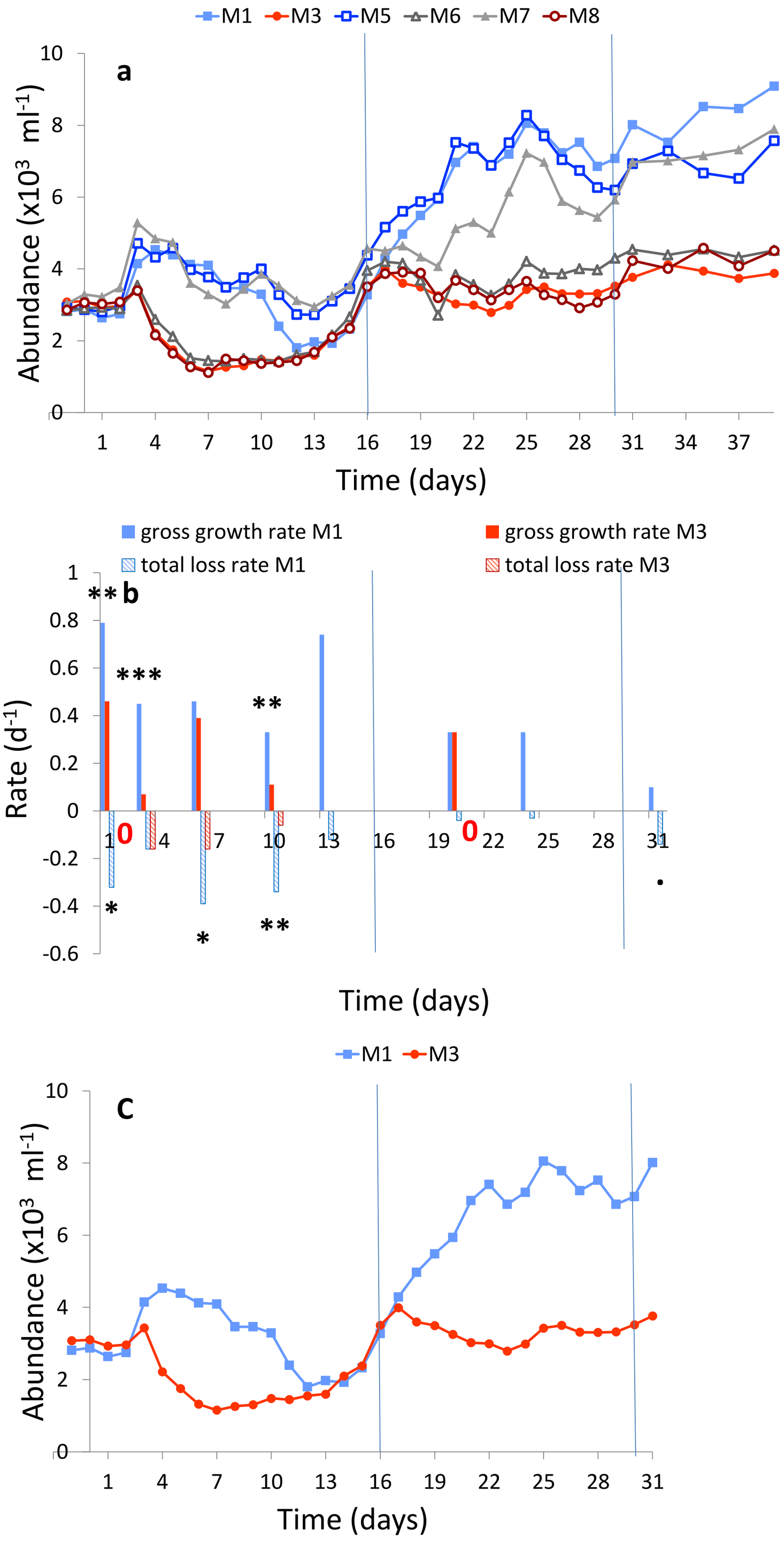
M1
M3
M5
M6
M7
M8
a
Abundance (x10³ ml⁻¹)
Time (days)
gross growth rate M1
gross growth rate M3
total loss rate M1
total loss rate M3
b
Rate (d⁻¹)
c
Abundance (x10³ ml⁻¹)
Time (days)
d
Net growth rate (d⁻¹)
y = -0.0006x + 0.61
R² = 0.94
fCO2 (µatm)
e
Abundance (x10⁴ ml⁻¹)
y = -6.3459x + 10549
R² = 0.91
fCO2 (µatm)

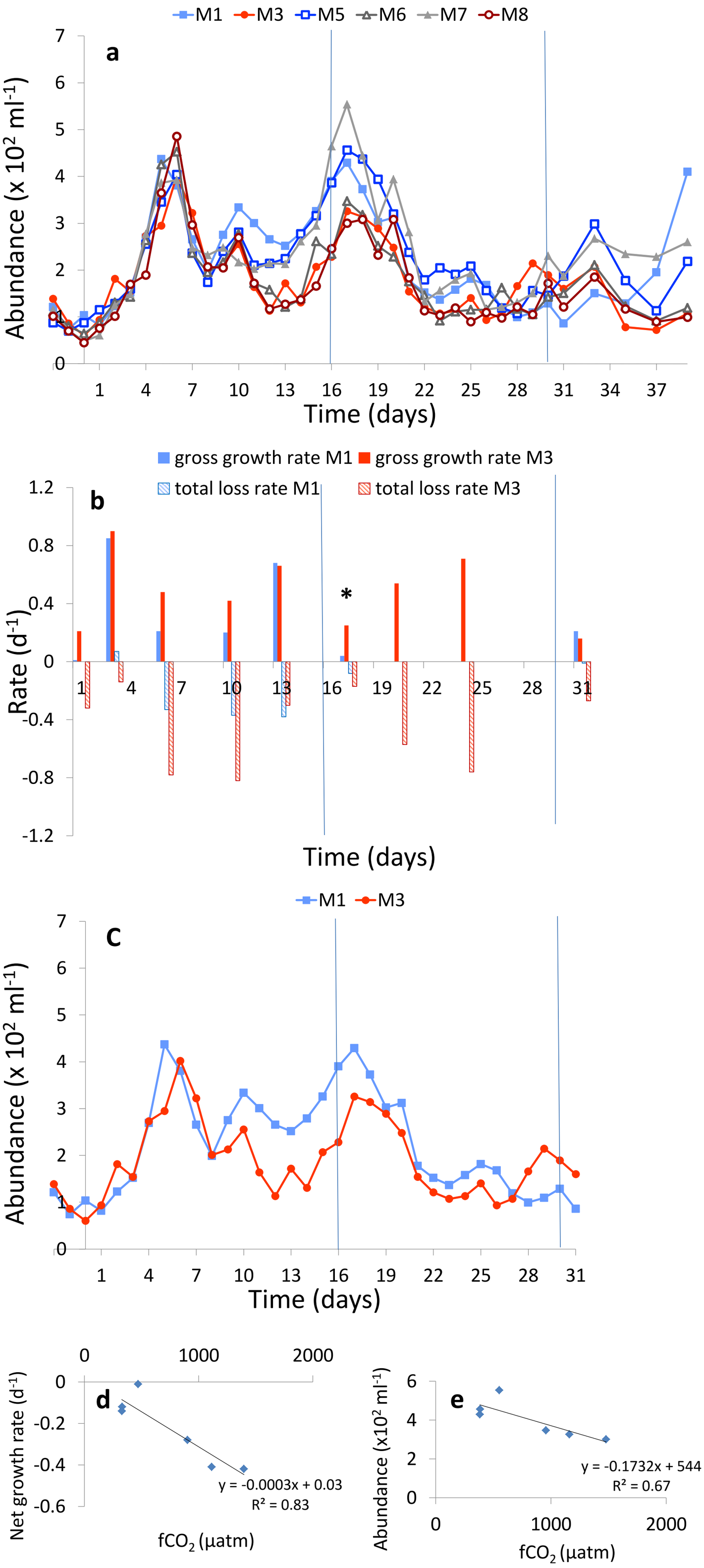
M1
M3
M5
M6
M7
M8
a
Abundance (x 10² ml⁻¹)
Time (days)
gross growth rate M1
gross growth rate M3
total loss rate M1
total loss rate M3
b
Rate (d⁻¹)
*
Time (days)
M1
M3
c
Abundance (x 10² ml⁻¹)
Time (days)
d
Net growth rate (d⁻¹)
y = -0.0003x + 0.03
R² = 0.83
fCO₂ (µatm)
e
Abundance (x10² ml⁻¹)
y = -0.1732x + 544
R² = 0.67
fCO₂ (µatm)

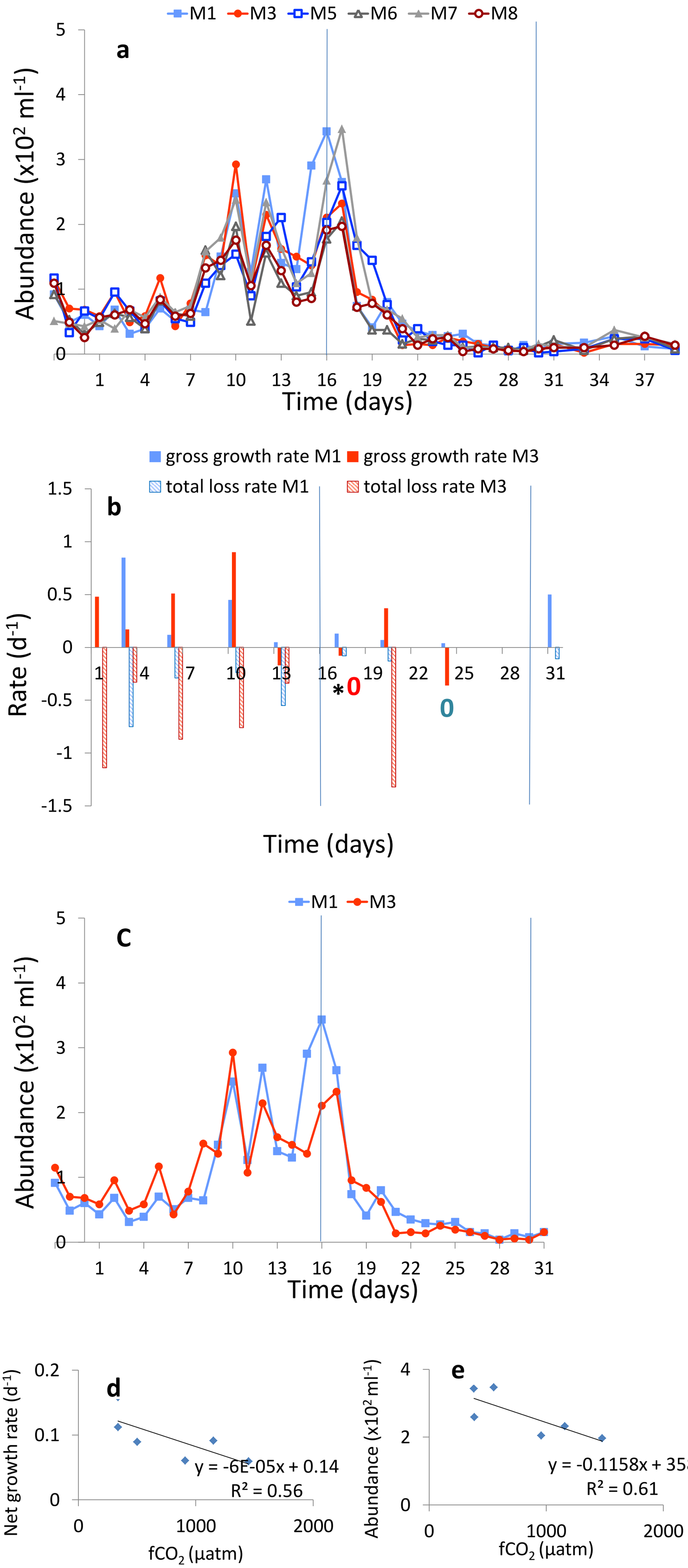
M1
M3
M5
M6
M7
M8
a
Abundance (x10² ml⁻¹)
Time (days)
gross growth rate M1
gross growth rate M3
total loss rate M1
total loss rate M3
b
Rate (d⁻¹)
*0
0
M1
M3
c
Abundance (x10² ml⁻¹)
Time (days)
d
Net growth rate (d⁻¹)
y = -6E-05x + 0.14
R² = 0.56
fCO₂ (µatm)
e
Abundance (x10² ml⁻¹)
y = -0.1158x + 358
R² = 0.61
fCO₂ (µatm)

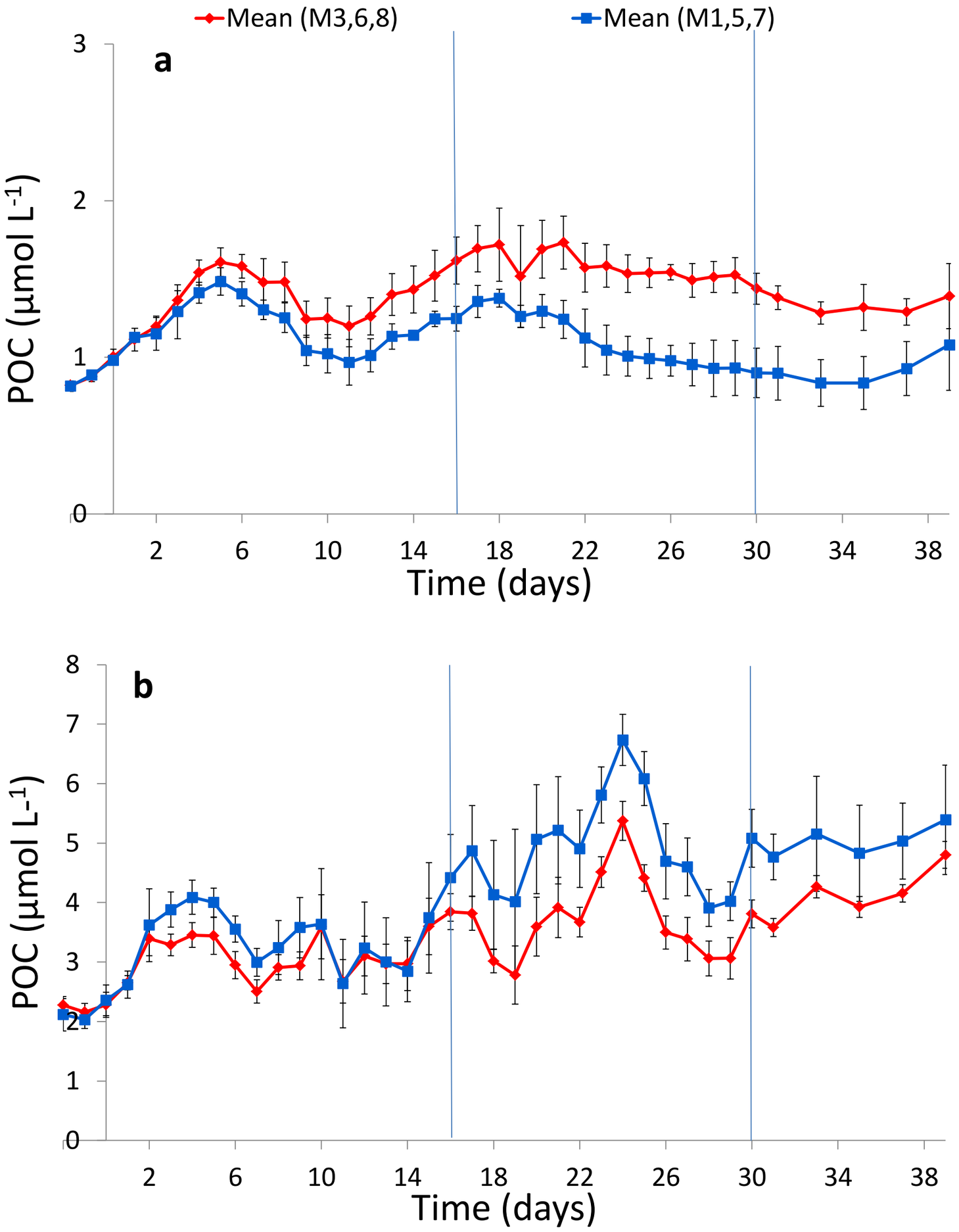
Mean (M3,6,8)
Mean (M1,5,7)
a
POC (µmol L-1)
0
1
2
3
2
6
10
14
18
22
26
30
34
38
Time (days)
b
POC (µmol L-1)
0
1
2
3
4
5
6
7
8
2
6
10
14
18
22
26
30
34
38
Time (days)

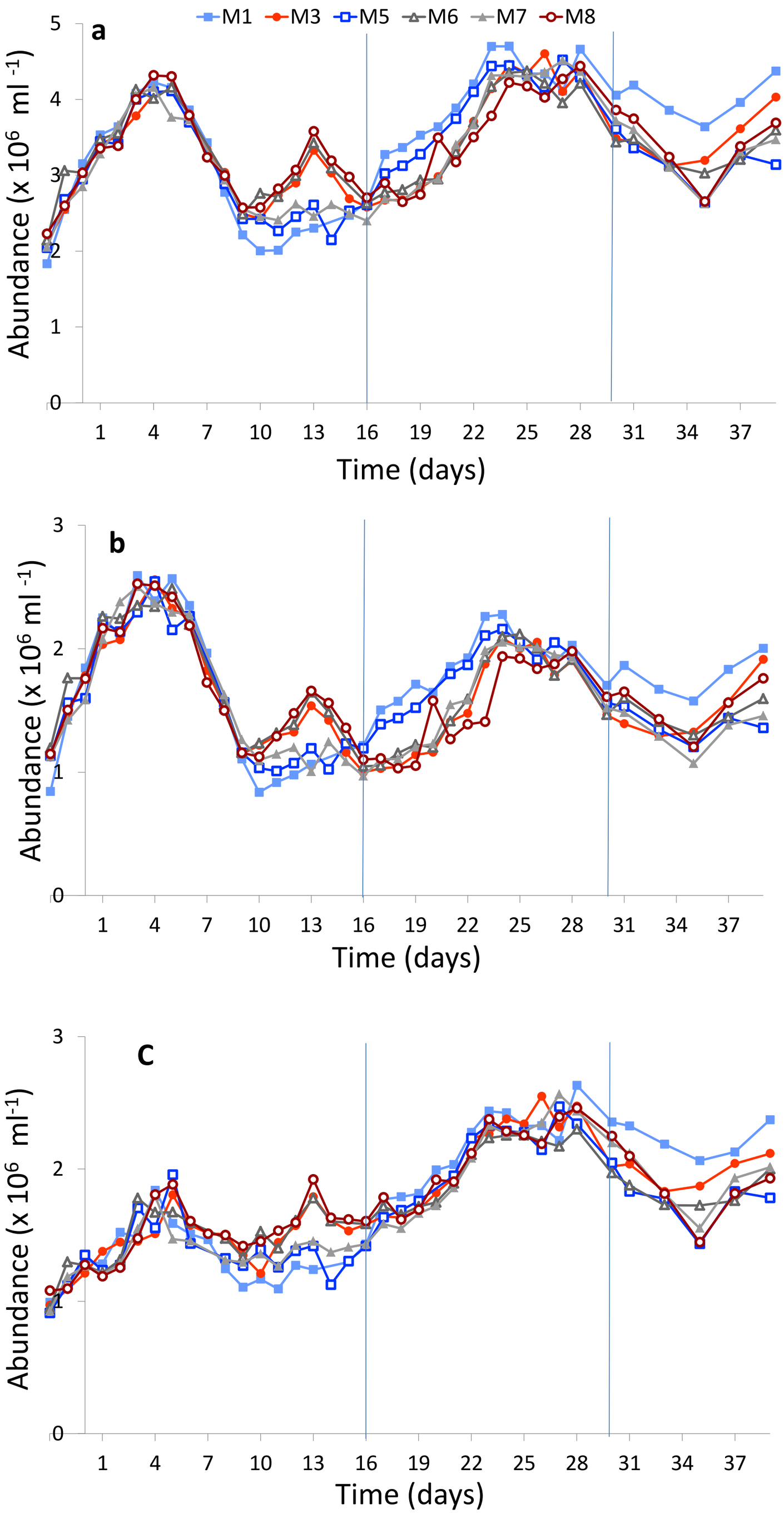
M1
M3
M5
M6
M7
M8
a
b
c
Abundance (x 10^6 ml^-1)
Time (days)
0
1
2
3
4
5
1
4
7
10
13
16
19
22
25
28
31
34
37

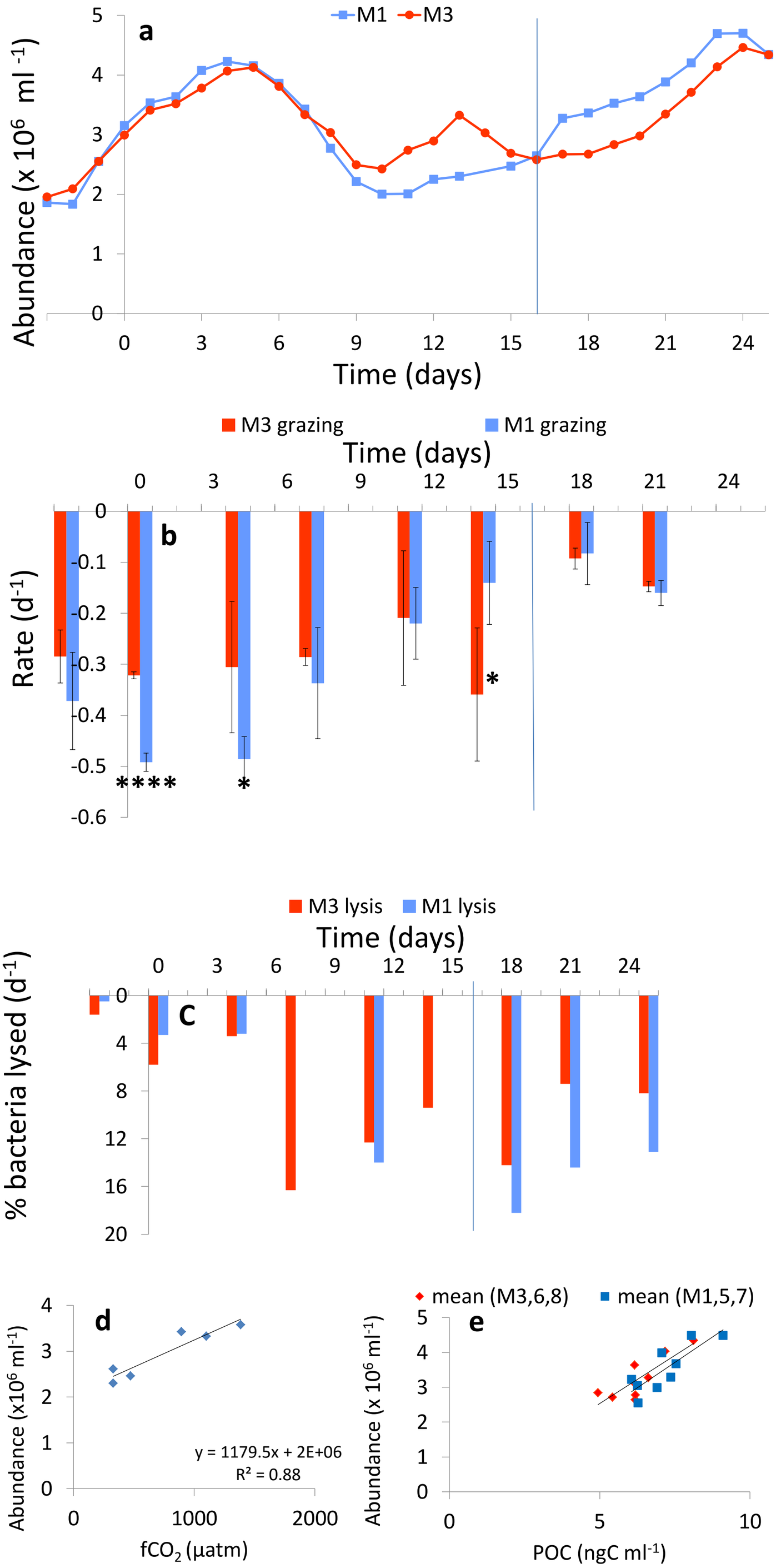
a
M1
M3
Abundance (x 10^6 ml^-1)
Time (days)
M3 grazing
M1 grazing
b
Rate (d^-1)
M3 lysis
M1 lysis
c
% bacteria lysed (d^-1)
d
y = 1179.5x + 2E+06
R² = 0.88
fCO2 (µatm)
e
mean (M3,6,8)
mean (M1,5,7)
POC (ngC ml^-1)

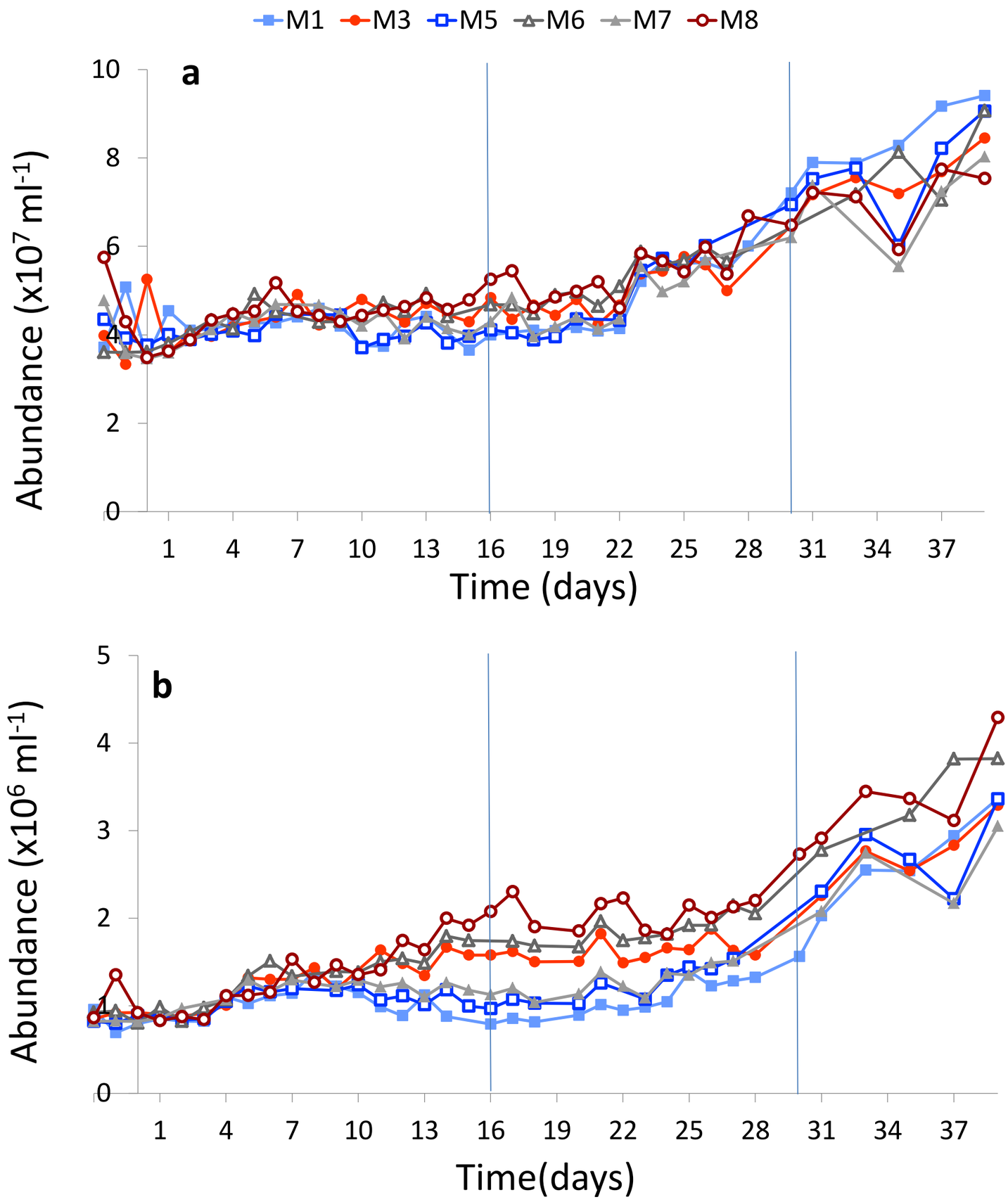
M1
M3
M5
M6
M7
M8
a
Abundance (x10⁷ ml⁻¹)
Time (days)
b
Abundance (x10⁶ ml⁻¹)
Time(days)